

5-15-2018

Structural Evolution and Regional Implications of the Arrowhead Mine Fault within the Pahranaagat Shear Zone, Nevada, USA

Michael Dennis Evans
mevansmusic@gmail.com

Follow this and additional works at: <https://digitalscholarship.unlv.edu/thesesdissertations>

 Part of the [Geology Commons](#)

Repository Citation

Evans, Michael Dennis, "Structural Evolution and Regional Implications of the Arrowhead Mine Fault within the Pahranaagat Shear Zone, Nevada, USA" (2018). *UNLV Theses, Dissertations, Professional Papers, and Capstones*. 3248.
<https://digitalscholarship.unlv.edu/thesesdissertations/3248>

This Thesis is brought to you for free and open access by Digital Scholarship@UNLV. It has been accepted for inclusion in UNLV Theses, Dissertations, Professional Papers, and Capstones by an authorized administrator of Digital Scholarship@UNLV. For more information, please contact digitalscholarship@unlv.edu.

STRUCTURAL EVOLUTION AND REGIONAL IMPLICATIONS OF THE ARROWHEAD
MINE FAULT WITHIN THE PAHRANAGAT SHEAR ZONE, NEVADA, USA

By

Michael Dennis Evans

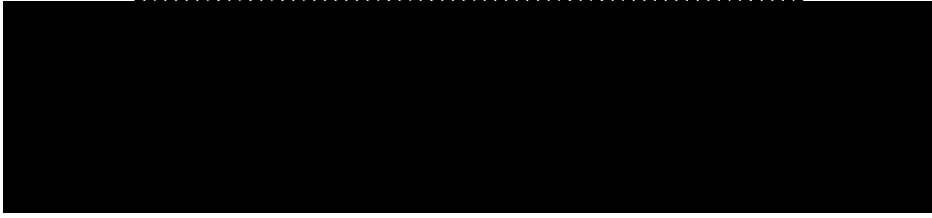
Bachelor of Science – Geology
California Lutheran University
2013

A thesis submitted in partial fulfilment of the requirements for the

Master of Science – Geoscience

Department of Geoscience
College of Sciences
The Graduate College

University of Nevada, Las Vegas
May 2018





Thesis Approval

The Graduate College
The University of Nevada, Las Vegas

May 10, 2018

This thesis prepared by

Michael Dennis Evans

entitled

Structural Evolution and Regional Implications of the Arrowhead Mine Fault within the Pahranaagat Shear Zone, Nevada, Usa

is approved in partial fulfillment of the requirements for the degree of

Master of Science – Geoscience
Department of Geoscience

Wanda Taylor, Ph.D.
Examination Committee Chair

Kathryn Hausbeck Korgan, Ph.D.
Graduate College Interim Dean

Rodney Metcalf, Ph.D.
Examination Committee Member

Ganqing Jiang, Ph.D.
Examination Committee Member

Barbara Luke, Ph.D.
Graduate College Faculty Representative

Abstract

STRUCTURAL EVOLUTION AND REGIONAL IMPLICATIONS OF THE ARROWHEAD MINE FAULT WITHIN THE PAHRANAGAT SHEAR ZONE, NEVADA, USA

By

Michael Evans

Dr. Wanda J. Taylor, Examination Committee Chair

Professor of Geoscience

University of Nevada, Las Vegas

The Basin and Range province is characterized by normal faults associated with extension, but the occurrence of strike-slip faults and the seismic hazard accompanying them is less understood. One major strike-slip zone, the Pahrnagat shear zone (PSZ), lies in Lincoln County, Nevada and within the boundary zone between northern Basin and Range (NBR) and central Basin and Range (CBR) sub-provinces. The PSZ is a 20-25 km long zone of Cenozoic left-lateral faults. The Arrowhead Mine Fault (AMF) is one of the three major faults in the PSZ. The western AMF and the faults that surround and abut it are the foci of this research. The purpose of this research is to understand the timing and style of deformation of the AMF, the PSZ, and the relationship of the PSZ to regional tectonics. I hypothesize that the AMF is a recent tectonic feature that supports a model of regional sinistral transfer between tectonic regimes. The best way to obtain the spatial and geometric data needed to address the issue was detailed mapping with

emphasis on fault cross-cutting, termination, and kinematic relationships at 1:12,000 scale of the western AMF and surrounding area in the East Pahranaagat Range. New fault data, and stereographic analysis of bedding and compaction foliation data along with cross sections and a fence diagram provide evidence that the normal faults and strike-slip fault are kinematically compatible and were active synchronously, indicating that the AMF is a transfer fault. Strike-slip fault splays form a flower structure/duplex that are shown to have formed synchronously with a number of normal faults in the area. Internally, the duplex contains both contractional and extensional structures, divided by a through-going fault. This situation is uncommon in models of duplex formation, but is suggested here to have formed during segment linkage.

Cross-cutting relationships indicate that the AMF cuts Kane Wash Tuff, Gregerson Basin Member, along one strand, constraining the age to ~15 Ma or younger. By constraining the age and style of deformation of the AMF we find that the PSZ was active late in the development of the NBR to CBR boundary zone.

The PSZ plays a distinct role in the intraplate tectonics of the region, falling within the Southern Nevada Seismic Belt. It may be facilitating strain transfer from other sinistral structures within the Southern Nevada Seismic Belt (Caliente-Enterprise Zone, Rock Valley Fault Zone, etc.). The presence of both a western termination of the AMF and a gap in left-lateral structures to the west suggest that the NBR-CBR boundary is still developing, which has implications for the interconnectivity of Walker Lane with the Intermountain Seismic Belt and has implications for seismic hazard.

Acknowledgments

The accomplishment of this project is due to the hard work and selflessness of many people who have given me their time and support. Here I take a moment to acknowledge all the people and organizations that have made this project possible. I want to first thank my adviser, Wanda J. Taylor, for her unending support, patience, advice, encouragement, and mentorship with this project and in my life. None of this research would be possible without her vision and problem solving. I would like to thank the members of my research group, including but not limited to: Thomas Price, Mahmud Muhamad, Shaimaa Abdelhaleem, Alexander Peck, and Rebecca Ely. In addition, it is important to acknowledge the contributions from my field assistants including: R. Alexis McIntyre, Max Hinson, Sam Albarran, and Jeremy Miera, among others. My parents, Steve Evans and Anne Alba, provided the encouragement and financial support to follow my dreams. Sara Gedo has been the emotional foundation for this work.

I also thank the Nevada Petroleum and Geothermal Society and the USGS EDMAP Program (Award No. G15AC00157 to W.J. Taylor) for their financial support for this project. My committee members, Drs. Metcalf, Jiang, and Luke, have also made this project possible. Maria Rojas and Liz Smith have helped ensure that I navigated the academic landscape. The UNLV Department of Geoscience has been an amazing and supportive family who continues to strive for academic excellence.

Table of Contents

ABSTRACT.....	iii
ACKNOWLEDGMENTS.....	v
LIST OF FIGURES.....	viii
CHAPTER 1	
INTRODUCTION.....	1
CHAPTER 2	
GEOLOGIC SETTING.....	5
CHAPTER 3	
STRATIGRAPHY.....	14
CHAPTER 4	
STRUCTURAL DATA AND MEHTODS.....	18
CHAPTER 5	
DISCUSSION.....	21
CHAPTER 6	
REGIONAL TECTONISM.....	28

CHAPTER 7

CONCLUSIONS.....	36
APPENDIX A: Point counts, fault data and station data.....	50
APPENDIX B: Geochronology.....	59
APPENDIX C: Plates.....	64
REFERENCES.....	65
CURRICULUM VITAE.....	71

LIST OF FIGURES

Figure 1. Location map of field area and related regional landmarks.....	40
Figure 2. Active seismic zones with earthquake epicenters show the spatial..... relation between the PSZ and the Southern Nevada Seismic Belt.	41
Figure 3. Regional Structure map showing notable geologic structures and..... relevant geographic locations in southern Nevada and southwest Utah.	42
Figure 4. Relationship of normal faults to strike-slip faults in transfer faulting Normal faults transfer their slip onto the strike-slip fault in a synchronous deformational event.	43
Figure 5. Types of duplexes (flower structures).....	44
Figure. 6. Stratigraphic column showing the names and ages of the..... Cenozoic ash-flow tuffs and the underlying buttress unconformity.	45
Figure 7. Stereographic plots of fault sets.....	46
Figure 8. Strain ellipsoid of simple shear.....	47
Figure 9. Mountain-front sinuosity showing that the steep hillside..... formed recently and may still be active.	48
Figure 10. Proposed model of duplex development containing both normal..... and reverse faults.	49

Chapter 1

Introduction

To better understand the development of the Basin and Range Province as a whole, it is necessary to understand the interactions of its sub-provinces and characterize the boundaries between them. The boundary zone between the northern Basin and Range (NBR) and central Basin and Range (CBR) is poorly understood. The timing and style of deformation in this zone are critical components to understanding how these tectonic sub-provinces interact with each other. Previous work along this boundary has been done on the left-lateral Caliente-Enterprise zone in the east (Jayko, 1990; Axen, 1998; Hudson et al., 1998), which constrained its timing of deformation to 18–14 Ma and style to sinistral shear with counter-clockwise vertical-axis rotation. The Pahrnagat shear zone (PSZ) also lies within the central NBR-CBR boundary zone and is a left-lateral strike-slip fault zone (Fig. 1). The PSZ contains three major sinistral faults: the Arrowhead Mine fault (AMF), Buckhorn fault and the Maynard Lake fault. Regional scale work has been done on the PSZ by Tschanz and Pampeyan (1970) and Jayko (1990, 2007), but no work has been published describing and analyzing the PSZ or the major strike-slip faults within it in detail.

The PSZ not only lies within the transition between NBR and CBR, but it is also part of a zone of major seismic activity known as the Southern Nevada Seismic Belt (Fig. 2) (Kreemer et al., 2010; dePolo and dePolo, 2012). It has been suggested that the Southern Nevada Seismic Belt links and allows strain transfer from the Intermountain

Seismic Belt to the Walker Lane/Eastern California shear zone (Fig. 2) (Kreemer et al., 2010). In addition to the PSZ, notable sinistral structures, such as the Caliente-Enterprise zone and Rock Valley fault zone, coincide with this seismic belt (Fig. 3). Examining the western AMF allows for analysis of the relationship it has with structures to the west. This connection has implications for intraplate tectonics and how strain is transferred from the plate boundary zones into seismic belts. The driving forces behind intraplate tectonics are poorly understood. Understanding how strain is transferred on a regional scale can be gained by identifying interconnected regional structures. Study of structures within this seismic belt also may be used in determining the seismic hazard that the faults pose to populations in southern Nevada.

The AMF is the northernmost major strike-slip fault in the PSZ and it has many associated normal faults. The relationship between the nearby normal faults and the AMF has not been studied in detail before. The study area covers about 10 km² around the western end of the AMF and contains Paleozoic carbonates along with Cenozoic ash-flow tuffs. This detailed examination of the AMF requires defining the number of deformation episodes and considering the styles of deformation associated with strike-slip faults including the development of transfer faults and strike-slip duplexes.

Strike-slip faults can be transfer faults that transmit slip from connected kinematically compatible dip-slip or oblique-slip faults. The classic transfer fault model has dip-slip fault systems terminating into the strike-slip fault, but slipping in the same deformational event (Fig. 4). Multiple transfer faults form transfer zones where discrete zones of strike-slip and oblique-slip faults, that in many cases, are oriented parallel or sub-parallel to

the extension direction (Faulds and Varga, 1998). Transfer zones commonly accommodate strain transfer between extensional domains of differing spatial distribution, timing and magnitude of extension. Previous work suggested that the AMF is a transfer zone (e.g., Jayko, 1990). The new geologic map data (Plate 1) allow further assessment of this interpretation.

Duplexes along strike-slip faults, are imbricate fault systems similar in geometry to dip-slip duplexes, but instead are apparent in map view (Woodcock and Fisher, 1985).

Strike-slip duplexes are well recognized and have been well studied (e.g., Root, 1990; Woodcock and Rickards, 2003; Cembrano et al., 2005; Mitchel and Faulkner 2009; Jensen et al., 2011). Woodcock and Fisher (1985) separated strike-slip duplexes into transtensional (extensional) and transpressional (compressional) duplexes (Fig. 5).

Transtensional duplexes are dominated by normal faults between the bounding fault strands and have associated subsidence within their core. In contrast, transpressional duplexes are dominated by reverse faults and have notable uplift within them. These systems are commonly controlled by restraining and releasing bends in the strike-slip fault geometry.

The strike-slip duplex model delineates flower structures in cross section.

Transtensional duplexes create negative flower structures with internal extension while transpressional duplexes create positive flower structures with internal shortening (Fig. 5) (Woodcock and Fisher, 1985). Traditionally strike-slip duplexes fall into one of these two categories and hybrid duplex systems are rarely reported. Study of less-common types of duplex system development is important for predicting and understanding the

geometry and orientation of fracture systems associated with strike-slip deformation.

The western AMF provides an opportunity to collect data on and model the development of a structurally complex, less common type of strike-slip duplex.

The purpose of this study was to identify the age and kinematics of the western AMF, model its development, compare it to the related regional extensional systems, and identify regional tectonic zones that may be in development. I present the results of new geologic mapping with emphasis on cross-cutting relationships and structural analysis along the western AMF. The goal of this research is fourfold: (1) Identify the age and kinematics of the western AMF and its temporal and kinematic relation to normal faults. (2) Create a model for the development of the strike-slip duplex along the western AMF. (3) Place the western AMF and the PSZ in the context of regional extensional systems. (4) Understand the left-lateral PSZ and its relations to other along strike left-lateral zones in the NBR-CBR boundary zone.

Chapter 2

Geologic Setting

Southern and central Nevada are characterized by multiple deformations; the region underwent thrusting during the Sevier Orogeny followed by Cenozoic extension. Two major Cenozoic sub-provinces of the Basin and Range occur in southern and central Nevada, the NBR and CBR. The transition between the NBR and CBR also spatially coincides with a zone of active deformation, the Southern Nevada Seismic Belt. The geologic history of the area is a framework for the interpretation of the AMF along with the PSZ and the role they play in regional tectonics.

Sevier Thrusting

Mesozoic-Eocene age thrusts and folds of the Sevier and associated central Nevada thrust belts occur in Paleozoic rocks exposed in southern and central Nevada (Fig. 3). These contractional structures are a result of retro-arc compression related to subduction of the Farallon Plate under the North American Plate (140 Ma-50 Ma) (Atwater, 1970; Dickinson, 2006). The Gass Peak thrust is exposed just to the south of the PSZ and was a major thrust in the contraction (Guth, 1990; Jayko, 1990, 2007). This Sevier-belt thrust correlates northward with the Mt. Irish-Golden Gate thrust to the north in the central Nevada thrust belt and the geospatial distribution of these thrusts is consistent with the left-lateral motion along the PSZ (Taylor et al., 2000). Paleozoic rocks exposed along the southern side of the AMF are considered, here, as part of the

Gass Peak footwall. Many parts of the Mesozoic thrusts and thrust sheets are unconformably overlain by Cenozoic ash-flow tuffs (Long, 2012).

Cenozoic Extension

The Basin and Range Province in the western United States has been a focus of much geologic study and has been divided into four major sub-provinces; Northwestern, Northern (NBR), Central (CBR) and Southern (SBR) (Jones et al., 1992; Wernicke 1992; Sonder and Jones, 1999; Lerch et al., 2007). These sub-provinces have distinct differences in basin elevation, geophysical signatures, stretching factor, and timing of extension across them. Only the northern and central sub-provinces are important to this study. The NBR is characterized by extension that began about 40-35 Ma, a SSW decrease in the age of Cenozoic volcanic centers, multiple episodes of extension, and increased mantle/crust buoyancy as the mantle became warmer, exploiting crust and mantle potential energy (Sonder and Jones, 1999; Dickinson, 2006). The CBR is characterized by extension that began ~15-10 Ma with limited volcanism and major strike-slip faults (Sonder and Jones, 1999). Additionally, the CBR has a higher stretching factor than the NBR (Wernicke et al., 1988). The extension is likely a result of the external stresses from the NBR and SBR, and their differences in strain rate and possibly thermal structure (Wernicke, 1992; Sonder and Jones, 1999; Rau and Forsyth, 2011). Sonder and Jones (1999) ascribed the strain differences as a contributing factor behind the differences in the sub-provinces.

Northern Basin and Range

NBR extension occurred on both high-angle normal faults and low-angle detachment faults with the latter accommodating higher magnitudes of extension. The faults tend to be concentrated into areas of high extension with low extension areas in-between them. One of the significant areas of high-magnitude extension in the NBR is in the Highland Range where the Highland and Stampede detachments are exposed (Fig. 3).

The Highland detachment formed after 18.5 Ma and dips to the west (Axen, 1998). The Stampede detachment is an east-dipping low-angle fault that is pre-30.6 Ma (Taylor and Bartley, 1992). The up-dip continuation of the Stampede detachment is the Seaman breakaway, which is exposed to the west. Farther west, Fryxell (1984) described two sets of low-angle normal faults in the Grant Range (Fig. 3): an older, east-dipping set of late Oligocene and late Miocene faults, and a younger set of west-dipping Pliocene to Quaternary faults. The older faults include the east-dipping Humboldt fault and the Troy Peak fault. The Troy Peak fault is an east-dipping normal fault that cuts an equivalent of the Shingle Pass Tuff, meaning the fault is younger than 26.4 Ma (Fryxell, 1984). The youngest fault in the Grant Range is the Little Meadows fault, which forms fault-line scarps in alluvial fans, suggesting a Quaternary age (Fryxell, 1984). The faulting in the Grant Range creates an area of low extension between it and the Seaman breakaway to the east.

Magmatism in the NBR migrated southward through time (Sonder and Jones, 1999; Best et al., 2013a, b, c). Notable volcanism in the region started around Late Eocene-

Oligocene in the north and ended to the south around the NBR-CBR boundary zone, where the PSZ lies (Best et al., 1993; Best et al., 2013a, b, c). Extension in the NBR may be partially driven by asthenospheric upwelling along with gravity driven collapse (Sonder and Jones, 1999; Best et al., 2013) although the relationship between magmatism and extension is not exclusive as some extension predates volcanism in the region. Most extension occurred in approximately north-south oriented belts that cross the southward progression of volcanism. Pre-volcanic extension occurred along the Stampede detachment system, extension was syn-volcanic in the Hiko and Highland ranges and was post- volcanic in the Hiko and Timpahute ranges, among other places (Taylor and Switzer, 2001).

Major calderas in southern and central Nevada were the sources for most of the numerous ash-flow tuffs that cover the region. Understanding these ash-flow tuffs is critical to the story of the NBR-CBR boundary because they cover much of the area and are commonly cut by faults like the AMF. The Caliente-Indian Peak caldera complex lies to the east of the PSZ, the Central Nevada caldera complex to the northwest and the Southwestern Nevada volcanic field to the west. Most of the tuffs in the PSZ were erupted from the Caliente-Indian Peak caldera complex along with the Central Nevada caldera complex. Isotopically dated tuffs from the Caliente- Indian Peak caldera complex have yielded ages of 36.0 Ma to 18.5 Ma (Best and Christiansen, 1991; Best et al., 2013a, b) and dates from the Central Nevada caldera complex range from 36.1 Ma to 18.57 Ma (Best and Christiansen, 1991; Best et al., 2013 a, b). The youngest tuff exposed along the AMF, the Kane Wash Tuff, was erupted from an isolated caldera that lies southeast of the PSZ, the Kane Springs Wash caldera. Previous work has shown

that the Kane Wash Tuff is cut by the major strike-slip faults and normal faults in the PSZ (Jayko, 2007; Muhammad, 2016). The Kane Wash Tuff has been dated at 14.7 Ma (Best and Christiansen, 1991; Scott et al., 1993; Best et al., 2013 a, b) and I present further isotopic dating in a following section.

Central Basin and Range

The CBR is marked by differences in elevation, magmatism and timing of extension in comparison to the NBR. Basin elevations in the CBR are noticeably lower than in the NBR averaging from ~2000-2200 feet (~610-670 meters). This contrasts with the ~4000-4500 feet (~1220-1370 meters) in the NBR. The basin elevations change in the NBR-CBR boundary zone, which contains the PSZ in its northern part.

An amagmatic zone is present in much of the CBR (Anderson et al., 2010; Rau and Forsyth, 2011). This zone is notable because it sits between the major sweeps of volcanism from the NBR, which sweeps to the south, and SBR, which sweeps to the north (Anderson et al., 2010; Rau and Forsyth, 2011). It has been suggested that this amagmatic zone may be a result of asthenospheric melt getting trapped at depth by the Castle Cliffs, Tule Springs, Mormon Peak, and other low-angle detachment systems because volcanism exists nearby in the Caliente caldera complex and the Kane Springs Wash caldera, which are on the edge of the region of extension related to those detachments.

In the CBR to the southwest of the PSZ, the Mormon Peak, Tule Springs, and Castle Cliff detachments have an oldest known deformation age of 18 Ma along the Castle Cliffs detachment (Fig. 3) (Bidgoli et al., 2015). The Tule Springs detachment has yielded apatite ages of 13 to 14 Ma, which indicate uplift at that time (Bigolli et al., 2015). The Mormon Peak detachment has rapid exhumation dates of 14 to 13 Ma and 7.1 to 5.8 Ma (Bigolli et al., 2015). Deformation migrated to the west through this system of detachments. Deformation has been observed in 15 to 12 Ma volcanic deposits, indicating that they remained active past eruptive activity in the area and confirming the previous dates (Axen, 1998). The deformation associated with these detachments reaches an upper crustal western boundary around 114° 40' W, near the Meadow Valley Mountains (Axen et al., 1990). Together this detachment system has approximately 55 km of extension along it (Axen, 1990; Bigolli et al., 2015), making it a major extensional system in the CBR. Hudson et al. (1998) suggest that these detachment faults feed slip into the Caliente-Enterprise zone. This detachment system plays a critical role in understanding the deformation in the Caliente-Enterprise Zone to the north and the PSZ to the northwest.

To the south of the western PSZ lies the Sheep Range breakaway, a system of normal faults that includes the Sheep Basin fault, the Wildhorse Pass fault and the Mormon Pass fault (Fig. 3) (Guth, 1990). These faults dip west, but have unknown dip magnitudes. Normal faults of the Sheep Range breakaway formed synchronously with the Horse Spring Formation, which contains Neogene fossils (Guth, 1990). The Sheep Range has about 33% extension based on a tilted-block model (Guth, 1990). To the south, this system is in close proximity to the Las Vegas shear zone, a major right-

lateral fault system, and may be influenced by both it and the PSZ given its geospatial positioning.

Rock Valley Fault Zone

The Rock Valley fault zone sits about 50 km to the southwest of the PSZ and within the NBR-CBR boundary zone. It is a left-lateral strike-slip fault zone about 4 km wide and ~40 km long that probably originated in late Oligocene time, but is presently active (O'Leary, 2000). The Rock Valley fault zone is separated from the PSZ by the Sheep Range detachment system. The Rock Valley fault zone has a regional strike of around 050° compared to the average 060° strike of the PSZ. The location of the Rock Valley fault zone on the boundary of the southern Walker Lane suggests a plate boundary related tectonic driving force behind its movement rather than other extensional structures in southern Nevada, which in turn suggests that the Walker Lane and its plate boundary controlled tectonics may be driving intraplate tectonics in southern Nevada.

Caliente-Enterprise Zone

The Caliente-Enterprise Zone is a 20-50 km wide and 120 km long zone of vertical-axis rotation and faulting that lies along the transition between the NBR and CBR in eastern Nevada and western Utah (Fig. 3). Near the PSZ and to the east, the Caliente-Enterprise Zone has been interpreted to be a broad left-lateral transfer zone that accommodated heterogeneously distributed Miocene extension (Hudson et al., 1998). Counter-clockwise rotation in this zone started between 18 Ma and 14 Ma, and

continued through late magmatism in the area and after (Hudson et al., 1998). This zone can be divided into three parts, each influenced by different regional structures and events. The eastern part follows or forms an east-west trending segment of the Colorado Plateau margin, the central part is dominated by the Caliente caldera complex and the western part interacts with the sinistral strike-slip faults in the PSZ (Axen, 1998). Maximum rotation is as high as 90° in the east part and decreases to 15° in the west, where the left-lateral strike slip faults of the PSZ accommodate much of the strain (Hudson et al., 1998). The Caliente-Enterprise Zone has been interpreted as a transfer zone by Jayko (1990, 2007) and Hudson et al. (1998). Hudson et al. (1998) suggested that large magnitude extension to the south along the Mormon Peak detachment likely reduced the amount of sinistral rotation in the central part of the Caliente-Enterprise Zone. The Caliente-Enterprise Zone may have acted as the southern boundary of NBR extension (Axen et al., 1993).

Another major left-lateral strike-slip fault near the Caliente-Enterprise zone and in the Southern Nevada Seismic Belt is the Kane Springs Wash Fault which has a strike of around 030°, compared to the average 060° strike of the PSZ. The Kane Springs Wash fault cuts, and thus, is younger than the Kane Springs Wash caldera and has Quaternary activity (U.S. Geological Survey and Nevada Bureau of Mines and Geology, 2006). In addition, the southernmost fault in the PSZ, the Maynard Lake Fault, has Quaternary fault scarps.

Southern Nevada Seismic Belt

The Southern Nevada Seismic Belt is an approximately E-trending band of seismicity that spans the Basin and Range province near 37°45'N latitude (Fig. 2) (Slemmons et al., 1965; dePolo and dePolo, 2012). Kreemer et al. (2010) provided continuous global positioning system data supporting the existence of an active shear zone in southern Nevada that links the Wasatch fault in the Intermountain Seismic Belt to the Eastern California Shear Zone/Walker Lane (Fig. 2). Geodetic data indicating 1.8 mm/yr of extension also supports this model of a zone of active seismicity which has been called the Southern Nevada Seismic Belt (Kreemer et al., 2010; dePolo and dePolo, 2012). The geospatial proximity of Caliente-Enterprise Zone to the Southern Nevada Seismic Belt, Quaternary fault scarps and modern seismicity suggest that the zones are tectonically related. Major sinistral structures in the NBR-CBR boundary zone fall within this seismic belt including the PSZ, Rock Valley fault zone and the Caliente-Enterprise Zone. These structures may be localizing deformation to the boundary zone.

Chapter 3

Stratigraphy

Paleozoic units in the area are shallow marine deposits, primarily carbonates that make up the basement on which Cenozoic tuffs are deposited. The major Paleozoic units in the field area include the Ordovician Eureka Quartzite and the Devonian Sevy Dolomite, Simonson Dolomite, and Guilmette Formation. These units are described in detail on Plate 1.

Unconformably overlying the Paleozoic units is a clast-supported conglomerate unit containing rounded clasts of Paleozoic carbonates. Small outcrops of fresh water limestone of an unknown age are present stratigraphically above the conglomerates. Due to the limited age constraints, the conglomerate is mapped as Cretaceous or Tertiary in age (Plate 1). The conglomerate has clast sizes ranging from large, well-rounded cobbles to small well-rounded pebbles and is poorly sorted with little matrix. It also contains cross beds and channels. The thickness of the unit varies along the unconformity. This thickness variation is interpreted to be a result of deposition against a paleohill along a buttress unconformity.

The Cenozoic section is composed of Oligocene and Miocene ash-flow tuffs that were erupted from nearby calderas including the Caliente caldera complex, central Nevada caldera complex and the Kane Springs Wash caldera (Fig. 6). Stratigraphy and phenocryst assemblages for the Cenozoic tuffs are shown on Plate 1. Thin sections

were point counted by me and compared to previous literature by Best et al. (1993) for unit correlation (Table 1, Appendix A). The PSZ lies in the distal area of distribution of regional tuffs sourced from the Central Nevada caldera complex including the oldest tuff, the 27.57 Ma Monotony Tuff. In contrast, the PSZ lies near the calderas for the 18.5 Ma Hiko Tuff and 14.7 Ma Kane Wash Tuff. Both of these situations lead to significant changes in unit thickness across the area.

Two units display significant thickness variations across the map area: the Hiko and Monotony tuffs. Field observations (Plates 1 and 2) indicate that the Hiko Tuff is thicker in the northwest and thins to the southeast, which is supported by other literature (Best et al., 2013a). The Monotony Tuff thickens at the AMF to 75 m from ~40 m to the north and the south. This suggests that a depositional basin or topographic low existed in the area near the AMF. The Monotony Tuff overlies the Tertiary-Cretaceous conglomerate and associated fresh water limestone. Together, the thickness change and the stratigraphic position suggest that a topographic low or paleohill existed in the area south and east of the exposures of Paleozoic rocks (Plate 1) that was partially filled with the ash-flow tuff, Monotony Tuff, allowing for greater thickness in the deepest part of the basin.

The point count data from thin sections generally agree with field identifications and previously published modal percent phenocryst analyses (Table 1, Appendix A) (Best et al., 1993; Scott et al., 1991) Of these point-count data, sample 15-1 is the only outlier in comparison to published point counts (Table 1, Appendix A) (Best et al., 1993). This sample has more quartz than shown by Best et al. (1993); however, Cook (1965)

reports a similar amount of quartz in the lowest Kane Wash unit. Stratigraphic positioning along with $^{40}\text{Ar}/^{39}\text{Ar}$ dating (see below) suggest that sample 15-1 is part of the Kane Wash Tuff, but further work needs to be done classifying the multiple cooling units of ash-flow tuffs within the Kane Wash Tuff.

The Kane Wash Tuff contains two members: the Gregerson Basin and the Grapevine Spring (Novak, 1984; Scott et al., 1993). Field observations of the Kane Wash Tuff in the study area suggest that it is the Gregerson Basin Member due to the phenocryst assemblage of about 2/3 sanidine and 1/3 quartz with a few percent of other minerals; a highly welded cap on the tuff; and a non-welded to partially welded, lithic-rich basal section. There have been several attempts to isotopically date the Kane Wash Tuff. Novak (1984) used K-Ar and obtained dates ranging from 15.7 ± 0.2 Ma to 14.1 ± 0.2 Ma. Scott et al. (1993) used more modern $^{40}\text{Ar}/^{39}\text{Ar}$ dating which yielded ages of 14.67 ± 0.22 Ma on the Grapevine Spring Member, and 14.39 ± 0.28 Ma and 14.55 ± 0.14 Ma on the Gregerson Basin Member. My new $^{40}\text{Ar}/^{39}\text{Ar}$ analysis of sanidine phenocrysts from the Kane Wash Tuff yielded a date of 15.13 ± 0.42 Ma (Appendix B). Thirteen sanidine crystals were analyzed from a sample collected from a site near part of the AMF at L4 (Plate 1), the same site as thin section 15-1. The ranges of dates, all isotopic data and probability distribution are shown in Appendix B. The data were dispersed over a range of dates with a slight grouping around 15.1 Ma. The results yielded a mean square weighted deviation of 1.9 with no isochron, meaning that the distribution of dates is “overdispersed”. These data have a larger scatter than statistically predicted, but are still useful for unit correlation because no other tuffs in the known section have an age within less than 3 m.y. of the Kane Wash Tuff. Variations in sanidine dates may indicate

that the phenocrysts may have not been in a closed system. While the 15.13 Ma date may have poor accuracy based on statistical analysis, it lies within the margin of uncertainty of the Scott et al. (1993) dates for Kane Wash Tuff. In addition, this new date is consistent with an $^{40}\text{Ar}/^{39}\text{Ar}$ analysis obtained from the Kane Wash Tuff several kilometers to the south that yielded a date of 15.3 +/- 0.09 Ma (Price, 2017). Taking into account uncertainty, all of the dates for the Gregerson Basin Member cluster around 14.7 Ma. The rock from which the sample was taken for dating of the Kane Wash Tuff is cut by a major strand of the AMF giving us a maximum age of last deformation around 14.7 Ma.

Chapter 4

Structural Data and Methods

All geologic map data were collected with traditional mapping techniques. One to twelve thousand scale topographic maps were used in the field to record contact and attitude data along with fault geometries and orientations. A geologic compass was used to measure fault orientations, bedding and compaction foliations. Compaction foliation and bedding data are shown in Table 3, Appendix A. Compaction foliation data is measured off of flattened pumice, fiamme, in the tuffs to represent the position of original horizontality. Compaction foliation and bedding data were used in conjunction with fault and contact data to construct a geologic map (Plate 1), cross sections (Plate 2), a fault timing map (Plate 3), and a fence diagram (Plate 4).

Fault Sets

The faults in the map area are divided into sets A-D based on strike and structural associations (Fig. 7; Plate 3). Fault set A (FA) is the oldest fault set in the area. These faults are characterized by striking NNE-SSW. FA strikes range from 024°-044° and includes 3 faults. Only one had a measurable dip (Fig. 7). FA is distinguished from other SW-NE striking faults in the area because Faults 1 and 2 are cross cut by Fault 3 in fault set B (FB) as seen at L1 (Plate 3). FB strikes 116°-173° (NW) and has dips ranging from 56°-74°. FB is cut by the younger fault set C (FC). FC strikes from 012°-056° (NNE). FC is the second set of faults that strike NNE-SSW, like FA does. FC is

differentiated from FA due to cross-cutting relationships of Fault 3, in FB, at L2 with Fault 4 of FC (Plate 3), making FA older than FB and FC. Fault set D (FD) is made up of the AMF and its related faults. The major faults of FD are the AMF and its two related splays; their strikes range from 042° to 075° . The AMF and related splays form a strike-slip duplex. Faults internal to the duplex strike from 171° to 247° and are normal, oblique and reverse faults. Measured 5° N slickenline rake data on a 039° striking fault (station #75) in FD indicates strike slip that is kinematically compatible with the AMF. All fault data are recorded in Table 2, Appendix A.

Faults of FD have orientations (ENE) and intersection geometries, fault topology, that suggest they are kinematically compatible with FC (NNE) indicating that they may have formed synchronously as a single fault network. It is expected that normal or reverse faults that form in the same deformational event as a strike-slip fault would have 90° or 45° orientations to it (Fig. 8). For example, at L3 (Plate 3) Fault 4 of FC forms a 45° angle with Fault 5 of FD which fits with Sylvester's (1988) simple shear models of kinematic compatibility in strike-slip systems (Fig. 8). In the northeastern part of the field area, two fault scarps in Quaternary alluvium were observed. These faults have a N-S strike and indicate that active deformation has occurred in the area.

Mountain Front Sinuosity

Mountain-front sinuosity was calculated along a western portion of the AMF (Fig. 9). Mountain-front sinuosity is a result of a balance between stream and slope processes that tend to produce a sinuous mountain front and active tectonics that tend to produce

a straight mountain front. Consequently, low values (1.01 to 1.14) suggest active mountain fronts (Bull and McFadden, 1977). The length of the fault surface trace was measured as was the length of a straight line across the same area (Fig. 9). The measured values are divided to estimate how recently the mountain front formed using the following equation: $Smf=Lmf/Ls$ where Smf is mountain front sinuosity, Lmf is the distance along the sinuous mountain hillslope – alluvial fan break and Ls is the straight line distance along the same mountain front. In this case, Smf came out to 1.0187 which indicates recent activity; however, bedrock lies close to the mountain front which can decrease the Smf value.

Chapter 5

Discussion

Paleogene Unconformity

The paleohill and Cretaceous-Tertiary conglomerate documented here represent regional paleorelief on the Paleogene unconformity, which was largely created during and after the late Jurassic-Cretaceous Sevier orogeny (e.g., DeCelles and Coogan, 2006; Long, 2012). The PSZ sits near the southeastern edge of the Nevadaplano, a high Sevier-hinterland plateau. The edge of the Nevadaplano may be marked, in this area, by the Gass Peak thrust, one of the major thrusts of the Sevier fold-and-thrust belt. The PSZ cuts across the Nevadaplano and the Gass Peak thrust. Therefore, high levels of paleo-erosion and relief would have occurred during Jurassic to Eocene. The conglomerate unit, TKs, formed during or after thrusting and plateau uplift, and was deposited on dipping Paleozoic units in topographic lows. The subrounded clast shape, up to cobble sized clasts, cross beds, and channels in TKs suggest that it was deposited in a fluvial system. Significant paleo-relief is also documented ~50 km to the west in the Pintwater Range (Fig. 3) by the deposition of similar pre-volcanic conglomerates that required a major river for deposition (Guth, 1990). These features suggest the possibility that a regional drainage system existed near the southern edge of the Nevadaplano. Deposition of the TKs ceased prior to or at the time of the eruption of Oligocene tuffs.

The paleo-hills and channels created by thrusting and erosion formed the surface onto which the Oligocene-Miocene ash-flow tuffs were deposited. The tuffs were deposited against the Paleozoic carbonates in a buttress unconformity with approximately 34° of slope in the study area (Plate 5). Paleorelief on the Paleogene unconformity at least partly controls the distribution of Oligocene-Miocene ash-flow tuffs and their respective thicknesses because they lap up onto topographic highs and flow into lows. As these tuffs flowed along the ground, their thicknesses were not great enough to cover some larger hills composed of Paleozoic units. The paleo-hill in the area was at least 1200 m tall from reconstruction, shown by retrodeformation along cross section B-B' (Plate 5). The freshwater limestone was most likely deposited in lakes or swamps on top of TKs before the emplacement of tuffs.

Local deformation and development of a strike-slip duplex

Three distinct Cenozoic deformations occurred based on fault set geometries, structural associations and cross-cutting relations of the four fault sets (Plate 2). Some fault timing is constrained by cross-cutting relationships between faults and Cenozoic tuffs of known ages. The first deformational event, D1, correlates with FA and is constrained by the cross-cutting relationship of FB. One fault in FA cuts units as young as Hiko Tuff (on the eastern edge of the map) and is overlapped by Kane Wash Tuff, so D1 occurred between 18.5 and 14.7 Ma. FB is associated with D2 and occurred between FA and FC/FD. These faults cut Hiko Tuff, but are not exposed near Kane Wash Tuff outcrops. Consequently, D2 clearly is younger than 18.5 Ma, but whether it is younger than 14.7 Ma is not known. D3 is related to FC and FD, including the AMF and its related normal

faults. These most recent sets of faults clearly cut Kane Wash Tuff making D3 younger than 14.7 Ma. Kinematic compatibility of faults in FC and FD suggests that they formed synchronously as a single fault network. Plates 3 and 4 show the fault geometries and my subsurface interpretations in cross sections and a fence diagram, showing the 3D interaction of the structures.

The new map data strengthen the previous implication that slip transfer occurs in the PSZ (e.g., Jayko, 1990). The spatial and geometric relations between normal faults in FC and strike-slip faults in FD, including the AMF, suggest that the AMF is a transfer fault, transferring slip from the normal faults along it (Fig. 4). Recent work by Muhammad (2016) suggests that the southernmost left-lateral strike-slip fault in the PSZ, the Maynard Lake fault, is also a transfer fault. This consistency suggests that the PSZ is a broad transfer zone, with multiple transfer faults within it.

The duplex along the AMF contains three strike-slip fault strands, with reverse faults predominant in the southern part of the duplex and normal faults prevalent in the northern part of the duplex; the main strand lies in the center (Plate 3). Cross section A-A' (Plate 1) shows the duplex system and the proposed geometries, where both positive and negative flower structures are visible in cross sectional view.

This duplex geometry is rarely reported and results in a distinctive geologic structure differing from more typical duplexes that contain only extensional (e.g., Cembrano et al., 2005) or only shortening structures (e.g., Woodcock and Rickards, 2003). Differences in internal deformation in different parts of the duplex are interpreted to be controlled by splay geometry. The southern duplex has a restraining bend, resulting in transpression,

and the northern part has a releasing bend, resulting in transtension (Plates 1 and 3). The duplex likely grew by either progressive propagation of new imbricate faults from the strike-slip fault, as typical strike-slip duplex systems commonly do (e.g., Woodcock and Fischer, 1986) or by the bending then linking of two propagating faults with a subsequent breakthrough fault. It is important to note that related imbricate faults may be referred to here as normal and reverse faults but actually have oblique slip rather than pure dip slip.

The intra-duplex faults between the AMF and the southeastern splay have oblique-reverse slip, which together with the right bend in a left-lateral fault suggests transpression along a restraining bend (Plates 1 and 4). This matches both real world (Woodcock and Fischer, 1986) and analog (Naylor et al., 1986) examples. Oblique-reverse faults in the duplex fit expected orientations in kinematically compatible strike-slip systems (Naylor et al., 1986; Sylvester, 1988), and therefore, likely formed in the same deformational event as this strand of the AMF.

Development of this restraining bend near the surface was most likely controlled by lithologic/rheologic constraints. The bend may have been created by the fault interacting with the Paleozoic carbonates in the paleohill rather than the surrounding tuffs. The carbonates are rheologically different from the Cenozoic tuffs. As the system propagated to the southwest (Fig. 5) through ash-flow tuffs it encountered the Paleozoic carbonates, which deform differently, causing the fault to bend around the paleohill by taking the path of least resistance. This interpretation suggests that the restraining bend is a relatively shallow feature and does not extend to great depth (Plate 4).

The northern duplex has a releasing bend geometry, resulting in transtension. This left bend in a left-lateral system fits traditional models of extensional duplexes where a releasing bend allows for extension within a strike-slip system, resulting in normal faulting within the duplex (Fig. 5) (Cembrano et al., 2005; Jensen et al., 2011). Normal faults in this duplex are kinematically compatible with the AMF, based on geometry and limited slickenline data. There are two significant normal faults in the northern duplex, one around 90° to the main strand of the AMF and the other around 40°. The orientation of these conjugate faults in the duplex match the conventional model of simple shear with normal faults forming within 45° of the strike-slip fault (Sylvester, 1988; Naylor et al., 1986) as shown in Fig. 8. This model has normal faults that accommodate irrotational bulk strain forming along the elongation axis related to the strike-slip fault, which matches observations on the AMF. The fault at 90° to the main strand may have been rotated within the duplex.

The development of the duplex can be interpreted in four stages (Fig. 10). The first stage started with two strike-slip faults propagating from the northeast and southwest. In the second stage, the northeastern fault propagated to the southwest and diverted its path around the rheologically different carbonates in the paleohill, resulting in a restraining bend. Early oblique-reverse faults may have formed at this time inside the restraining bend as a response to the change in strain distribution. The southwestern strand propagated to the northeast and created a releasing bend most likely in response to changes in local stress field caused by the restraining bend to the south. In the third stage of deformation, the northeastern and southwestern splays continued to propagate and associated intra-duplex faults continued to form. An oblique-normal fault formed in

the north in proximity to the releasing bend while oblique-reverse faults continued to move near the restraining bend. This set of oblique-reverse faults propagated eastward starting the formation of a breakthrough strike-slip fault in the center of the duplex. A second smaller splay along the southern strike-slip fault may have also formed during this time. After the formation of the restraining and releasing bends, the final stage in duplex development was the breakthrough of the main strand of the AMF. The main strand formed in response to strain within the duplex and oblique-slip faults forming in the center of the system that broke through the duplex. The breakthrough of faults allowed slip transfer slip from associated faults.

Quaternary Deformation

In addition to the recorded seismicity in the region, mountain-front sinuosity and fault scarps suggest relatively recent fault movements. The low mountain-front sinuosity of $S_{mf} = 1.0187$ suggests that the AMF is relatively young and may be active. Four areas of Quaternary faults may impact the AMF. To the north of the AMF and within the map area, two N-S striking Quaternary fault scarps are exposed in Qoa, consistent with modern seismicity in the area (Plate 1) (Kreemer et al., 2010). Quaternary faults have been noted to the northwest of the west end of the AMF, in Badger Valley (Fig. 3) (Anderson, 1999). These unnamed faults of Badger Valley have angles between 90° and 45° to the AMF. These orientations when considered in relation to the AMF suggest that the AMF has the potential to slip during movement along any of these Quaternary faults. The southernmost fault in the PSZ, the Maynard Lake Fault, is also noted as active in the USGS Quaternary Fault Database (U.S. Geological Survey and Nevada

Bureau of Mines and Geology, 2006) and by Muhammad (2016). In addition, at least one minor scarp in the Pahranaagat Valley underwent slip in the last 0.01-1.6 Ma (Anderson, 1999). Together the regional seismicity in the Southern Nevada Seismic Belt (Fig. 2), the active faults in the region, and the geometric relations between the AMF and the active normal faults suggest that the PSZ is still active. Consequently, the PSZ poses a seismic hazard to nearby communities, a prospect that merits study.

Chapter 6

Regional Tectonism

Regional detachment systems

The PSZ appears to be regionally influenced by detachment faults during Oligocene-Miocene time, creating strike-slip faults in a regional slip transfer zone along the NBR to CBR boundary. The detachment systems account for much of the Cenozoic extension and differences among them are likely the main structural influences on the PSZ and boundary zone between the NBR and CBR. The Highland detachment to the north; Mormon Peak, Tule Springs, and Castle Cliff detachments to the southeast; and the Sheep Range breakaway and associated detachment system to the southwest are the major documented Miocene low-angle normal fault systems, and thus, high-magnitude extensional regions, that lie in appropriate positions to influence the PSZ (Fig. 3) (e.g., Bidgoli et al., 2015; Guth, 1981, 1990; Guth et al., 1988; Hudson et al., 1998). To the north, the Highland detachment is a west-dipping low-angle normal fault with last known motion after the 18.5 Ma emplacement of the Hiko Tuff, the youngest tuff in the section in that area (Axen, 1998). Its age is similar to the PSZ with motion after 14.7 Ma and/or to the earliest normal faulting in the area (FA). To the southeast, the Mormon Peak, Tule Springs, and Castle Cliff detachments have an oldest known deformation age of 18 Ma in the Castle Cliffs, while the youngest known uplift age of the Mormon Peak detachment is 7-8 Ma based on zircon and apatite (U-Th)/U thermochronometry, recording rapid exhumation (Bidgoli et al., 2015).

The major Miocene detachment faults to the north and south of the PSZ accommodate different amounts of extension. Approximately 55 km of extension occurred among the Mormon Peak, Tule Springs, and Castle Cliff detachment faults (Axen et al., 1993; Bigolli et al., 2015). This extension may accommodate decreased rotation in the central Caliente-Enterprise Zone (Hudson et al., 1998). To the west, the Sheep Range breakaway was active during Miocene time based on the association of sedimentary megabreccia deposits within the Horse Spring Formation (Guth, 1981, 1990; Guth et al., 1988). To the north, extension across the Highland detachment ranges from ~10 km in the north to ~3.7 km in the south (Axen, 1998).

The geospatial distribution of the Caliente-Enterprise Zone; Mormon Mountain, Tule Springs, and Castle Cliff detachments; and Sheep Range detachment create a low extension zone to the south of the PSZ, centered in the northern Sheep Range (Fig. 3). Assuming a constant 10°W dip of the Mormon Peak detachment (e.g., Bigdoli et al., 2015), the Mormon Peak detachment meets the surface expression of the west-dipping breakaway fault of the Sheep Range detachment, the Sheep Basin Fault, at a depth of ~13 km, giving it the potential for ductile deformation. This ductile deformation may be a critical factor in the development of the near-surface low-extension zone. The PSZ with its high-angle normal faults and left-lateral strike-slip faults may allow strain to bypass the low extension zone by transferring it from the Sheep Basin Fault onto the PSZ.

The major detachment systems in the south, the Mormon Peak, Tule Springs and Castle Cliffs detachments, do not continue to the north past the Caliente-Enterprise Zone and cannot be correlated to detachment systems in the north like the Highland and Stampede detachment, due to differences in fault dip directions and fault numbers.

This suggests that the southern detachments transfer their slip into the Caliente-Enterprise Zone where sinistral slip and rotation accommodates the strain from these major structures. Then as the zone narrows to the west, slip is transferred onto the PSZ as sinistral strike-slip deformation. Strain west of the Sheep Range is also transferred into the PSZ through those major fault systems. In the north, strain from the Highland and Stampede detachments was transferred into the Caliente-Enterprise Zone with an area of low extension in the Seaman and Golden Gate ranges, and then high extension to the northwest in the Grant Range.

In the NBR, another area of low extension occurs in the Timpahute and Mt. Irish ranges between zones of high extension, which further demonstrates this aspect of extension. High-magnitude extension occurs to the east, along the Stampede and Highland detachments and to the west along to a number of low-angle normal faults in the Grant Range (Fryxell, 1984; Long, 2014). To the east of this low-extension zone, the ~15 Ma (<18 Ma) Highland detachment is similar in age to the PSZ (Axen, 1998). Fryxell (1984) describes two sets of low-angle normal faults in the Grant Range: an older, east dipping set of late Oligocene and late Miocene faults and a younger set of west-dipping Pliocene to Quaternary faults. The faulting in the Grant Range creates an area of low extension between it and the Seaman breakaway to the east. Although the PSZ is separated from the Grant Range by structures of the Timpahute lineament, the geospatial and temporal distribution of these features correlate with the PSZ and these faults may be regionally genetically linked to motion along the PSZ.

All of these detachments faults fit into the bigger picture of NBR vs CBR extension, showing a greater overall stretching factor on low-angle normal faults in the CBR than in the NBR (Wernicke, 1992). The PSZ accommodates this difference in regional magnitude and distribution of extension. In addition, the left-lateral PSZ is necessary to accommodate the different strain rates in the extensional regimes: faster in the CBR from slower, but with longer duration, in the NBR. The PSZ acted and may still be acting as a transfer zone with multiple transfer faults within it (i.e., AMF and Maynard Lake fault). The PSZ transfer zone is more localized onto a small number of faults than the Caliente-Enterprise Zone.

Strike-slip zones in the region

Nearby strike-slip faults include two major left-lateral zones that flank the PSZ, the Rock Valley fault zone to the southwest and the Caliente-Enterprise Zone to the northeast, along with the nearby Kane Springs Wash fault (Fig. 3). This series of strike-slip fault zones lies within the Southern Nevada Seismic Belt which has many strike-slip earthquake focal mechanisms and connects the Intermountain Seismic Belt to the east with Walker Lane and the Eastern California Shear Zone to the west (Kreemer et al., 2010; dePolo and dePolo, 2012). These faults and earthquakes represent a major zone of sinistral deformation.

The Rock Valley fault zone is a left-lateral strike-slip fault zone about 4 km wide and located about 50 km to the southwest of the PSZ (Fig. 3). It probably originated in late Oligocene time, but is presently active (O'Leary, 2000). The Rock Valley fault zone is interpreted to be an active, extensional domain boundary within the Walker Lane that

concentrates extensional strain between the Spring Mountains domain on the south and the volcanogenic terrane to the north (O'Leary, 2000). The Rock Valley fault zone may be a zone of strain transfer from the Walker Lane/Eastern California shear zone eastward into the Southern Nevada Seismic Belt. The connection between the Walker Lane/Eastern California shear zone, the Rock Valley fault and the southern Nevada seismic belt is an integral component of the intraplate neotectonics in southern Nevada.

The Caliente-Enterprise zone has been interpreted as a transfer zone in order to explain the vertical axis rotation and its westward decrease, which is consistent with my interpretation of the nearby PSZ transferring strain past a low-extension zone to the south. Although most data on the Caliente-Enterprise zone records Miocene maximum ages of deformation, the modern seismicity suggests that it is possible that deformation has continued into modern times or may have begun a second stage of modern activity. The Caliente-Enterprise zone's close geospatial proximity to the Southern Nevada Seismic Belt and modern seismicity zone suggest that the two zones are tectonically related.

The Kane Springs Wash fault is a left-lateral strike-slip fault that has a strike of around 030° , compared to the average 060° strike of the PSZ. Ekren et al. (1977) indicated that this fault displays horizontal slickenlines and has about 8 km of offset based on offset rhyolitic lava flow rocks. Pampeyan (1993) indicated about 4.5 km of left-lateral offset of the Kane Springs Wash caldera by the Kane Springs Wash fault. Quaternary fault scarps estimated to be <750,000 years old occur along most of the fault (U.S. Geological Survey and Nevada Bureau of Mines and Geology, 2006). This fault

represents sinistral deformation extending out of the Caliente-Enterprise zone, possibly transferring strain to other regional structures.

The Rock Valley fault zone, Caliente-Enterprise zone, Kane Springs Wash fault, and PSZ are all located along the NBR-CBR boundary zone and are part of a greater left-lateral strike-slip system that may be transferring strain from the Intermountain Seismic Belt to the Eastern California Shear Zone/Walker Lane (e.g., Kreemer et al., 2010). A gap in left-lateral faults along this zone exists in the Desert Hills and Desert Range, between the PSZ and Rock Valley fault. The Plutonium Valley accommodation zone also has a NE strike and lies between the PSZ and the Rock Valley fault, at least partially filling the gap (Figs. 2 and 3). This accommodation zone has a broad zone of tilted blocks that may represent a system of relay ramps (Guth, 1990), further supporting the model of a sinistral structural zone along the NBR-CBR boundary zone. The formation of the Rock Valley fault zone and Caliente-Enterprise Zone in the Oligocene and their association with Walker Lane/Eastern California shear zone and the Intermountain Seismic Belt suggest that these structures may have formed prior to the younger PSZ and Kane Springs Wash fault. All of these faults together represent the development of a broad left-lateral zone within the Southern Nevada Seismic Belt. The PSZ may have developed more recently to accommodate the transfer of strain across central part of the province.

These zones of sinistral strain are separated by some normal faults now in the area between the western PSZ and the eastern Rock Valley fault, but a strike-slip fault in this area is lacking (Fig. 3). It is possible that this lack represents the infancy of a major sinistral shear system across southern Nevada, connecting the Walker Lane to the

Intermountain Seismic belt through the Southern Nevada Seismic belt along the NBR-CBR boundary zone. The PSZ may continue to propagate to the west or a new set of sinistral structures may form to link these zones of deformation in the future. This model of regional tectonics would allow direct, hard strain transfer from the Walker Lane/Eastern California shear zone to drive seismicity in southern Nevada and western Utah.

Walker Lane is partially controlled by the Pacific-North American Plate interaction (e.g., Faulds et al., 2005) which in turn influences the Rock Valley fault zone and the Southern Nevada Seismic Belt. This connection suggests that plate boundary forces influence active seismic zones far from the plate boundary like the Southern Nevada Seismic Belt and that intraplate tectonics may, at least in part, be driven by plate boundary motions.

Earthquake focal mechanisms, *in situ* stress measurements and geodetic data support a WNW-ESE strain direction for modern extension, consistent with left-lateral deformation on ~ENE-oriented structures like the PSZ, western Caliente-Enterprise zone and Rock Valley fault zone in the Southern Nevada Seismic Belt (Zoback et al. 1981; Kreemer et al., 2010). The southernmost strike-slip fault in the PSZ, the Maynard Lake fault, is active and moved less than 130,000 years ago based on a Quaternary fault scarp in older Quaternary alluvium (U.S. Geological Survey and Nevada Bureau of Mines and Geology, 2006; Muhammad, 2016). This evidence of young deformation is consistent with the interpretation that the PSZ is part of a broader zone of left-lateral deformation within the Southern Nevada Seismic Belt and contains the structures that are responsible for the modern seismicity and deformation.

The new data presented here show evidence of deformation after 14.7 Ma along the AMF, but it is not clear how this deformation is related to modern seismicity. Either two distinct periods of deformation may have occurred or older deformation may have continued into modern times. Current data is not sufficient to reach a conclusion on the timing or number of deformational events younger than 14.7 Ma. Recent seismic activity in the PSZ with left-lateral strike-slip focal mechanisms suggests that the PSZ is currently active (Kreemer et al., 2010; dePolo and dePolo, 2012). Some of this seismicity may relate to faults that cut the Quaternary deposits in the study area and to the AMF. A system of sinistral shear structures through the Southern Nevada Seismic belt matches previous models of an active shear zone in the region (Kreemer et al, 1010) although a gap in sinistral structures in the Desert Hills and Desert Range, between the PSZ and Rock Valley fault, suggests that this system may be still in development.

Chapter 7

Conclusions

This research on the AMF and PSZ addresses local and regional scale problems in fault system development, regional strain transfer and intraplate tectonics along the NBR-CBR boundary.

- The deformational history along the AMF consists of at least three deformational events (D1-D3) along four sets of faults. The AMF formed in D3, which is composed of the kinematically compatible fault sets FC and FD.
- The AMF (FD) is a transfer fault with kinematically compatible normal faults (FC) that transfer slip across them onto the strike-slip fault.
- The western AMF provides a unique example of duplex development and fault linkage. This duplex contains distinct zones of both transtensional and transpressional structures, which is not explained by standard models. I suggest a model with step-wise development of a restraining bend followed by a development of an overlapping releasing bend and then breakthrough of a straighter fault. Rheologic differences in subsurface lithology resulted in a restraining bend in the southern part of the duplex that facilitated compression. The northern part of the duplex formed normal faults in a releasing bend.
- The entire PSZ is a transfer zone in which all three major sinistral strike-slip faults transfer slip from their related normal faults. Transfer zones are composed of multiple transfer faults. In this case, the AMF and the Maynard Lake fault (Muhammad, 2015) are both transfer faults within the zone. The PSZ is likely

accommodating differences in timing, geospatial distribution and magnitude of extension between the NBR and CBR.

- This transfer zone was active after 14.7 Ma and possibly as recently as Quaternary. Both the AMF and Maynard Lake fault cut the Kane Wash Tuff, and the Maynard Lake fault displays Quaternary offset. In addition, the area is seismically active.
- The relations among the PSZ and the regional low-angle normal fault systems that influence it, suggest regional strain transfer across the NBR-CBR boundary zone and possibly Southern Nevada Seismic Belt. This transfer zone accommodates differences in timing, distribution and stretching factor between the NBR and CBR. The older and smaller offset Highland detachment in the NBR transfers strain southward onto the transfer zone. The Castle Cliffs, Tule Springs, Mormon Peak detachments along with the Sheep Range detachment systems have higher offsets and transfer that strain northward from the CBR. The spatial distribution of these fault systems and the presence of the transfer zone results in a zone of relatively low extension in the Sheep Range along the western PSZ. The multiple low-angle normal faults in the CBR facilitate a higher stretching factor than the few in the NBR during the same time and the difference is accommodated by the transfer zone.
- The Miocene to Quaternary(?) boundary between the NBR and CBR is a left-lateral transfer zone. The boundary zone is composed of the Caliente-Enterprise zone, the PSZ, the Rock Valley fault, and the Plutonium Valley accommodation

zone; however a gap in left-lateral faults across the zone between the AMF and the Rock Valley fault suggests that the transfer zone may still be developing.

- A maximum age of 14.7 Ma for the AMF combined with its close proximity to active Quaternary faults, low mountain-front sinuosity and the presence of seismicity in the region, suggests that the AMF accommodates Quaternary deformation.
- The Southern Nevada Seismic Belt is spatially coincident with several major left-lateral structures, including the PSZ, that likely facilitate strain transfer between major zones of active seismicity on a regional scale. The presence of modern seismicity in conjunction with a gap in left-lateral faults across the zone between the AMF and the Rock Valley fault suggests that the transfer zone may still be developing.
- The Rock Valley fault zone is a domain boundary within the Walker Lane/Eastern California shear zone (O'leary, 2000) and may be transferring strain from the Walker Lane/Eastern California shear zone to the Southern Nevada Seismic Belt. The Walker Lane is partially controlled by the Pacific-North American Plate interaction (e.g., Faulds et al., 2005) which in turn influences the Rock Valley fault zone and the Southern Nevada Seismic Belt. This connection has implications for our understanding of intraplate tectonics, suggesting that plate boundary forces influence active seismic zones far from the plate boundary, like the Southern Nevada Seismic Belt.

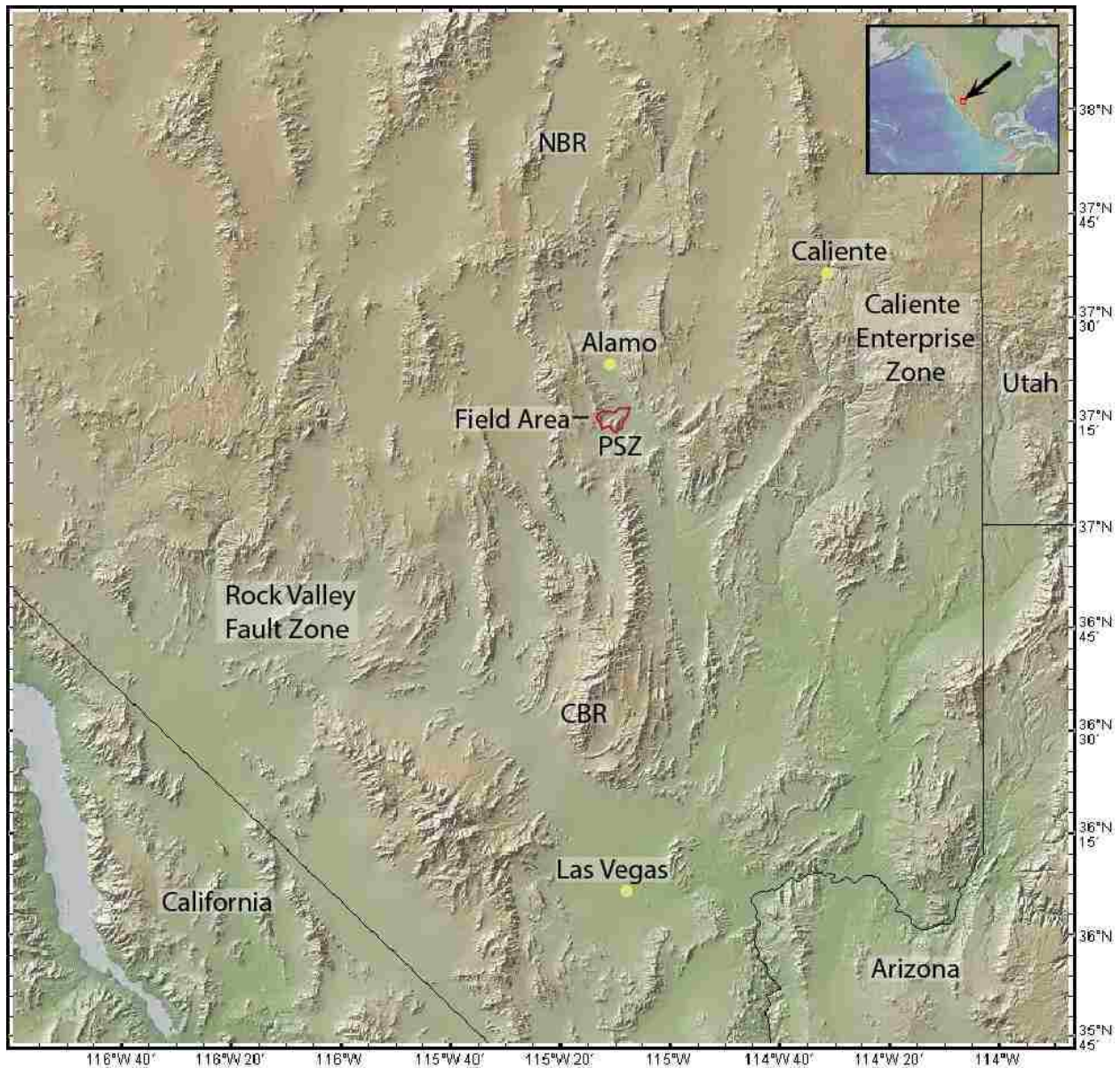


Figure 1. Location map of field area and related regional landmarks. The zone of changes in basin elevations, represented here by a change from green to tan, generally corresponds to the NBR-CBR boundary zone. Note the placement of the field area between the NBR and CBR and the differences in elevation across this boundary.

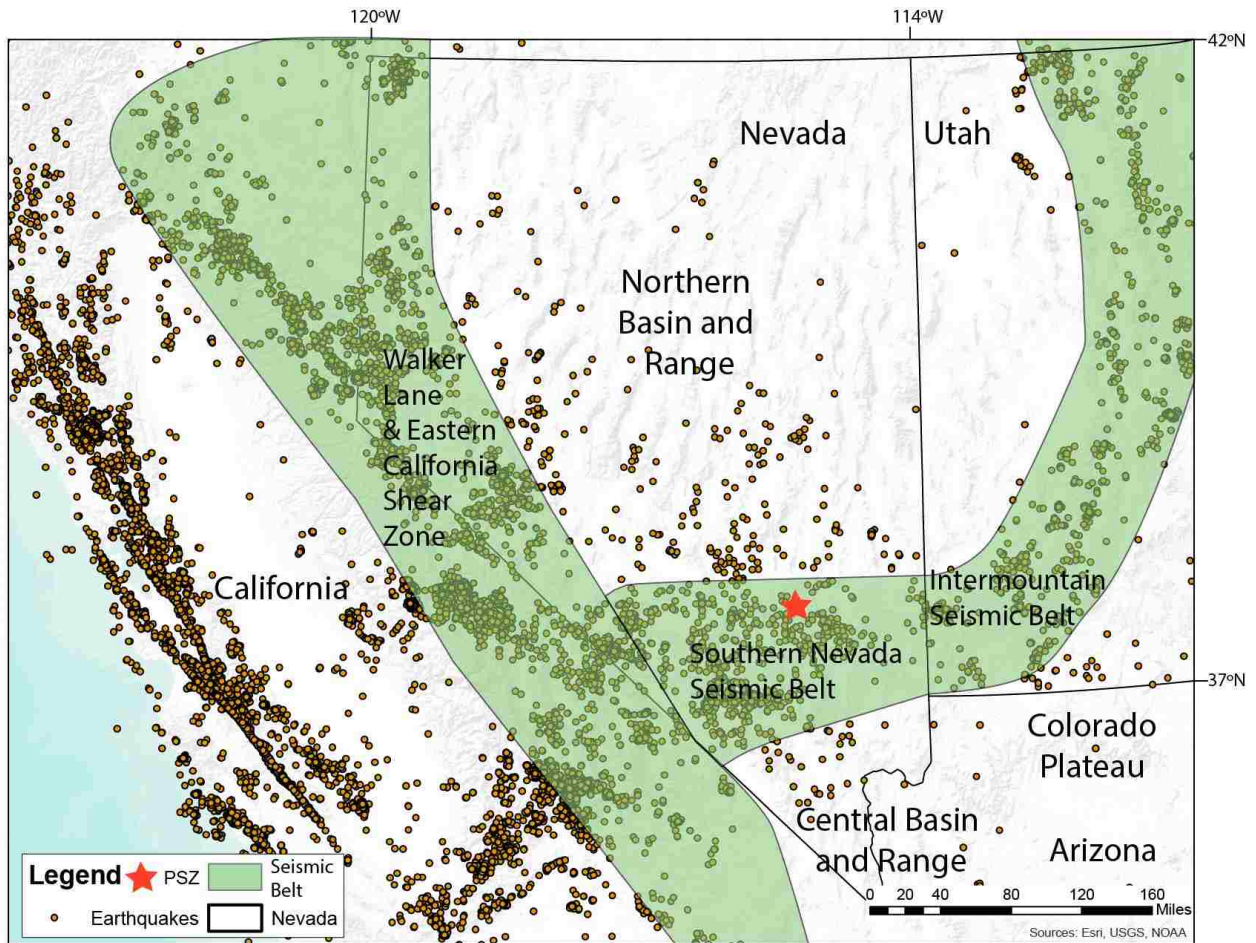


Figure 2. Active seismic zones with earthquake epicenters show the spatial relation between the PSZ (red star) and the Southern Nevada Seismic Belt. Shaded green areas show active seismic belts. The southern Nevada Seismic Belt connects the Walker Lane/Eastern California Shear Zone and the Intermountain Seismic Belt. Point data show magnitude 0.5 to 4 earthquakes between May 2014 and May 2015. Data was collected by the USGS and plotted in ESRI ArcMap.

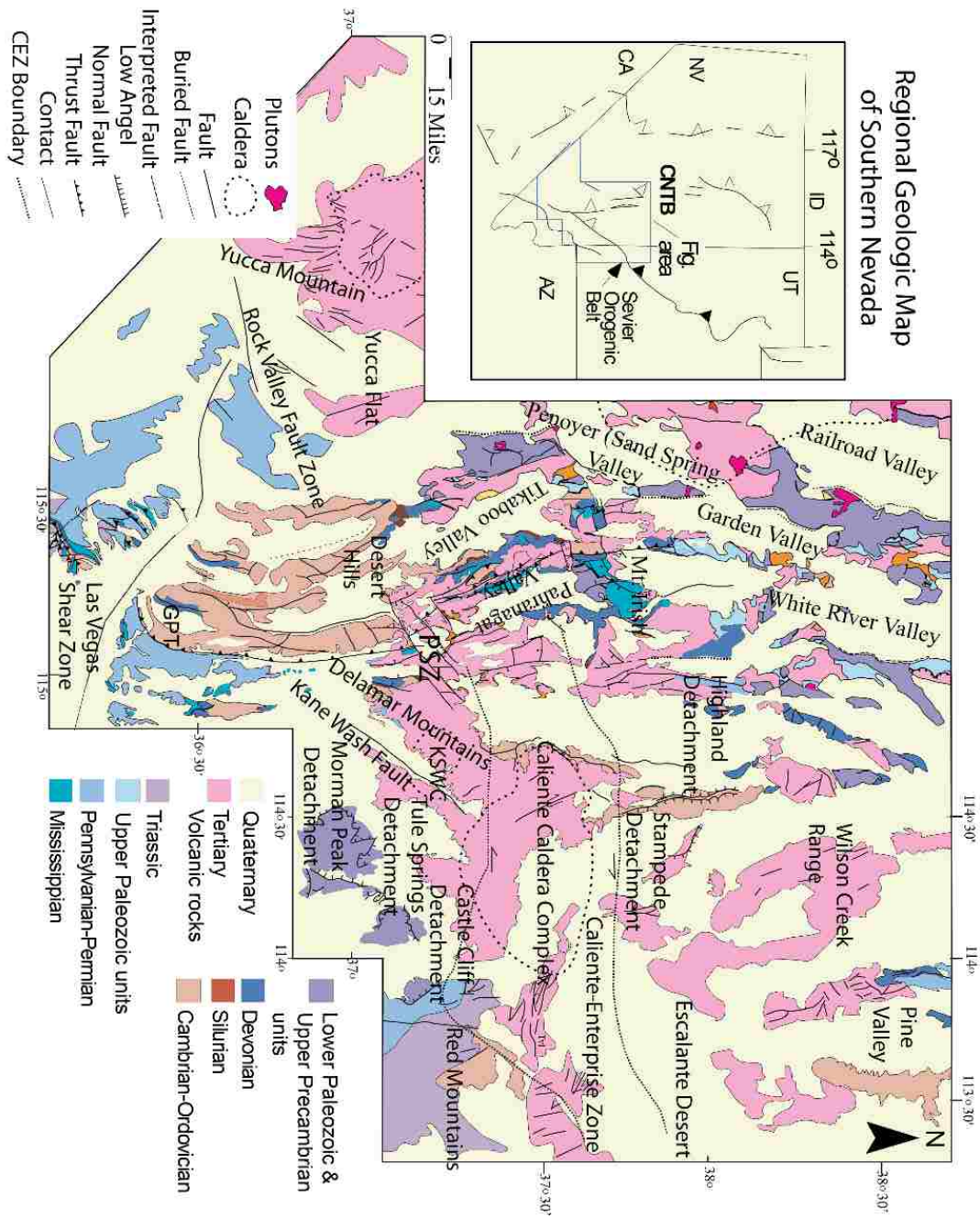


Figure 3. Regional geology map showing larger structures and simplified geologic units. PSZ – Pahranaगत shear zone, KSWC – Kane Springs Wash Caldera, GPT – Gass Peak Thrust, CNTB – Central Nevada Thrust Belt.

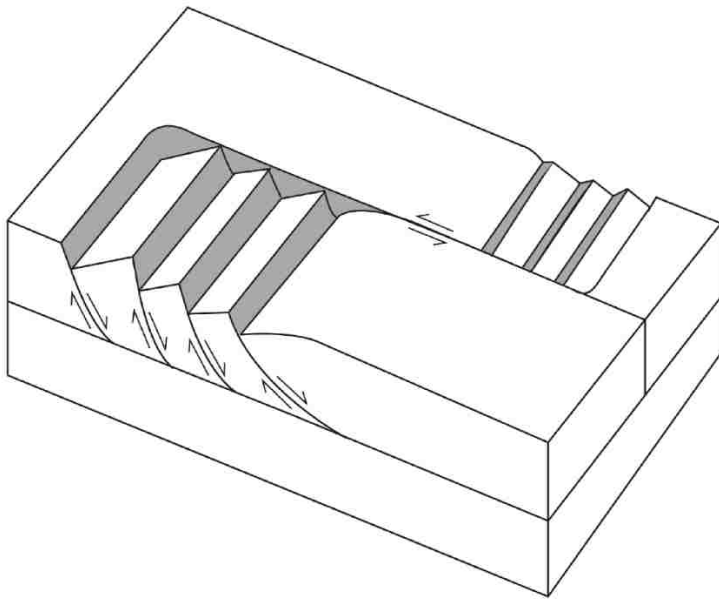


Figure 4. Relationship of normal faults to strike-slip faults in transfer faulting. Normal faults transfer their slip onto the strike-slip fault in a generally synchronous deformational event. Note the through-going strike-slip fault, which is the transfer fault.

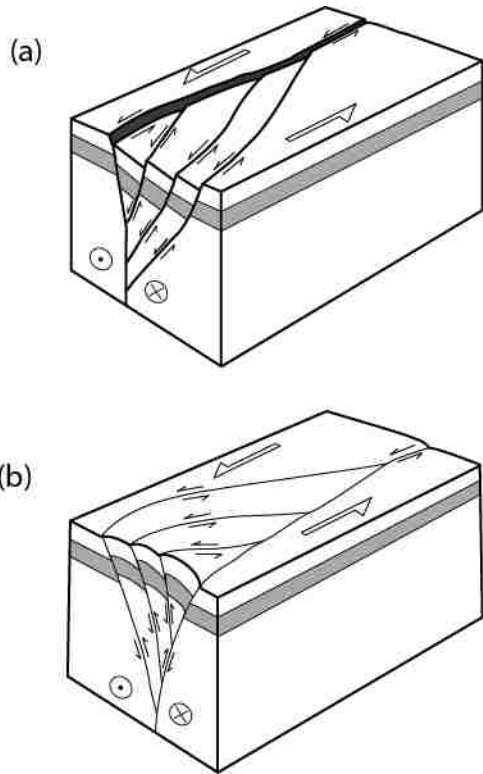


Figure 5. Types of duplexes (flower structures). (a) Transpressional duplex or negative flower structure in a left-lateral strike-slip system. Note the depression above the duplex body due to extension and normal faults. (b) Transtensional duplex or positive flower structure in a left-lateral strike-slip system. Note the uplift above the duplex body due to compression and reverse faults.

Cenozoic Stratigraphic Column

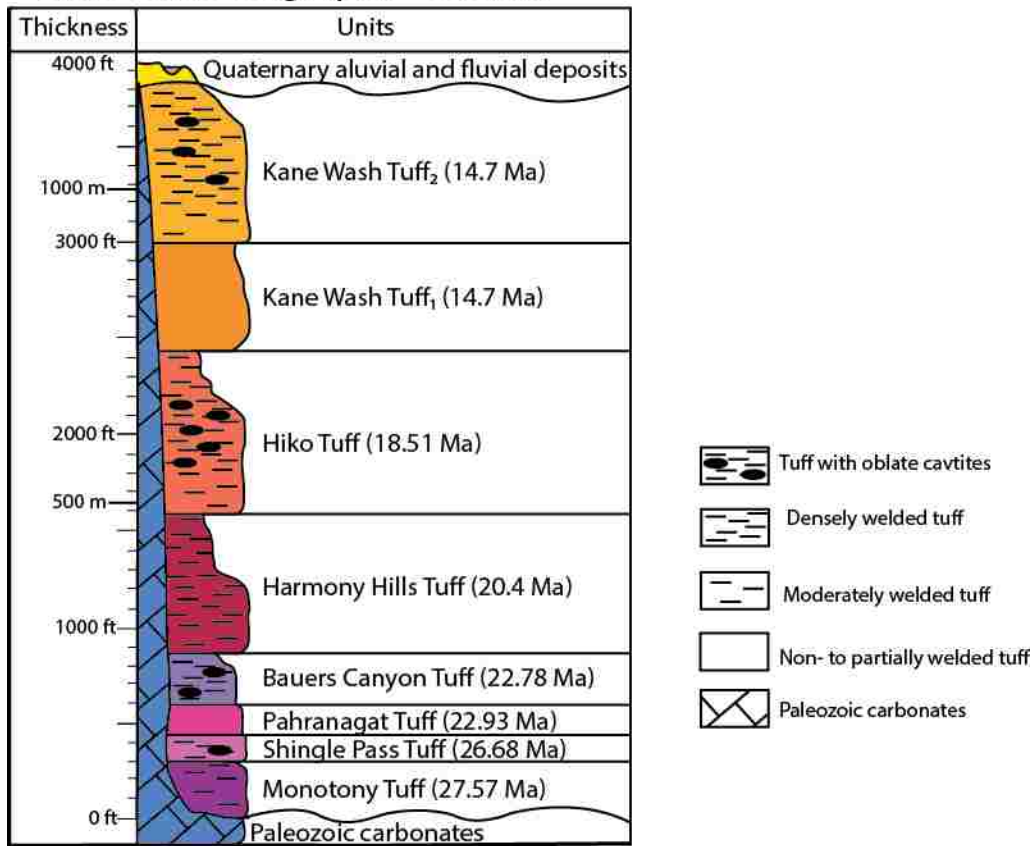


Figure. 6. Stratigraphic column showing the names and ages of the Cenozoic ash-flow tuffs and the underlying buttress unconformity. Paleozoic units, undivided, are shown in blue.

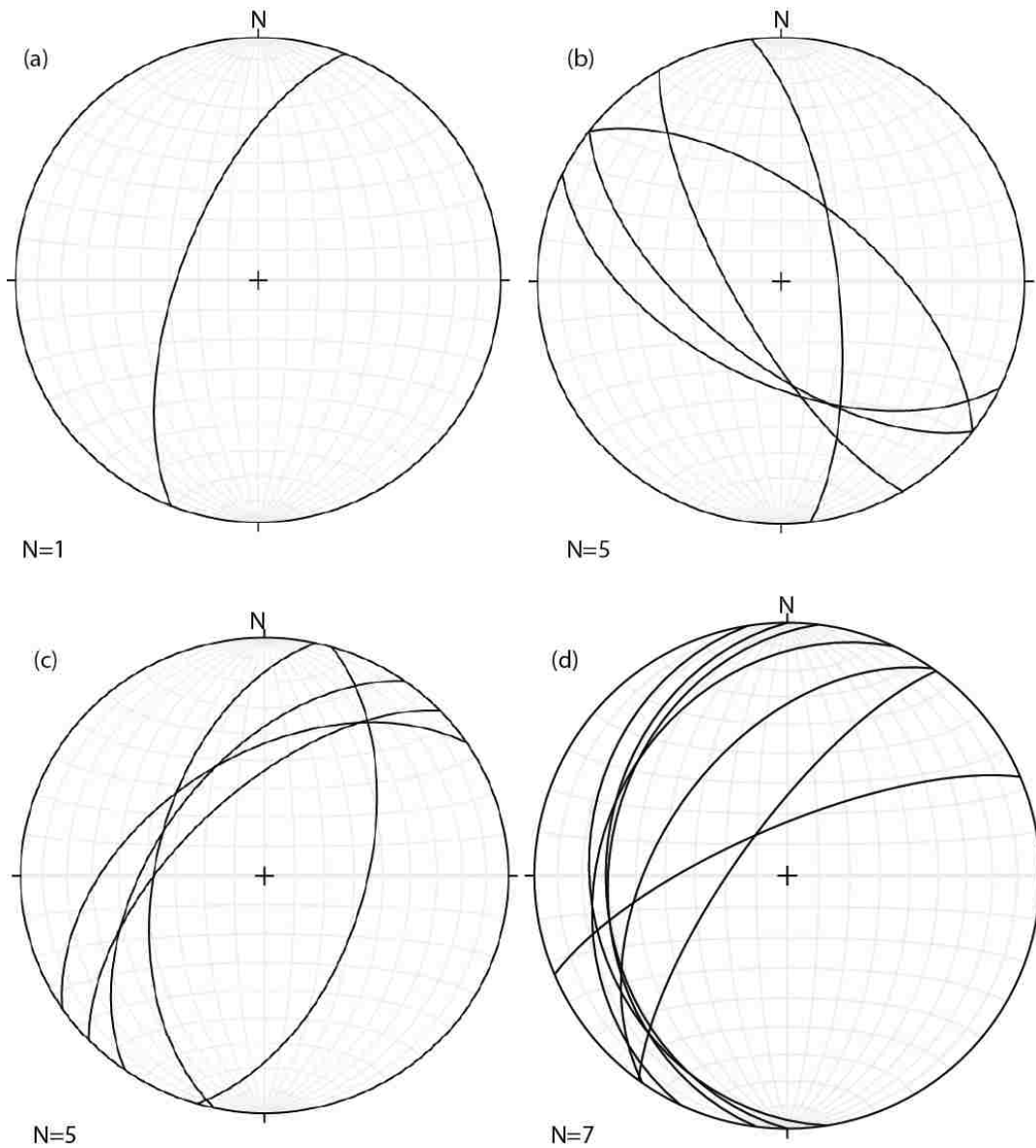


Figure 7. Stereographic plots of fault sets. N = number of measurable faults. (a) Fault A (FA) is the oldest fault. It has a NE-SW strike and is differentiated from other fault sets by cross-cutting relationships. (b) Fault set B (FB) cross cuts FA and is cut by FC. All faults in this set have a general NW-SE strike direction. (c) Fault set C (FC) is younger than FB and has general NE-SW strike direction. (d) Fault set D (FD) contains the AMF, its duplex and its related faults. The general strike direction of FD is NE-SW. Note similarity to FC suggesting kinematically compatibility. These fault sets may represent a single deformation event.

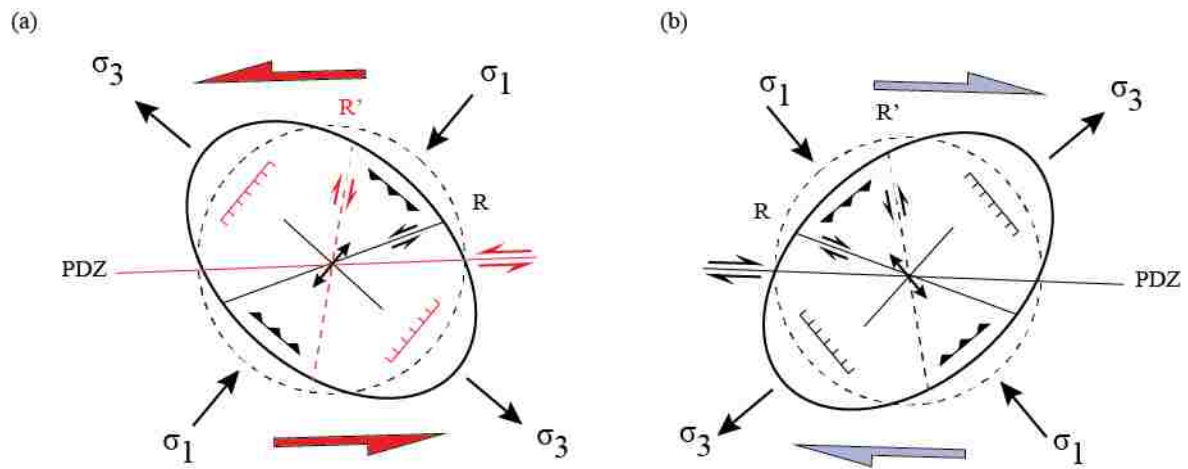


Figure 8. Strain ellipsoid of simple shear. (a) Sinistral shear. (b) Dextral shear. σ_1 = maximum stress; σ_3 = minimum stress; R = synthetic shears; R' = antithetic shears; PDZ = Principal deformation zone. Modified after Sylvester (1988) and Abdelhaleem (2015).



Figure 9. Mountain-front sinuosity showing that the steep hillside side formed recently and may still be active. L_s represents the length of the straight line while L_{MF} represents the length of the mountain front. By dividing the two, the mountain-front sinuosity, S_{mf} , is determined. S_{mf} is a representation of how much the mountain front has eroded since its creation.

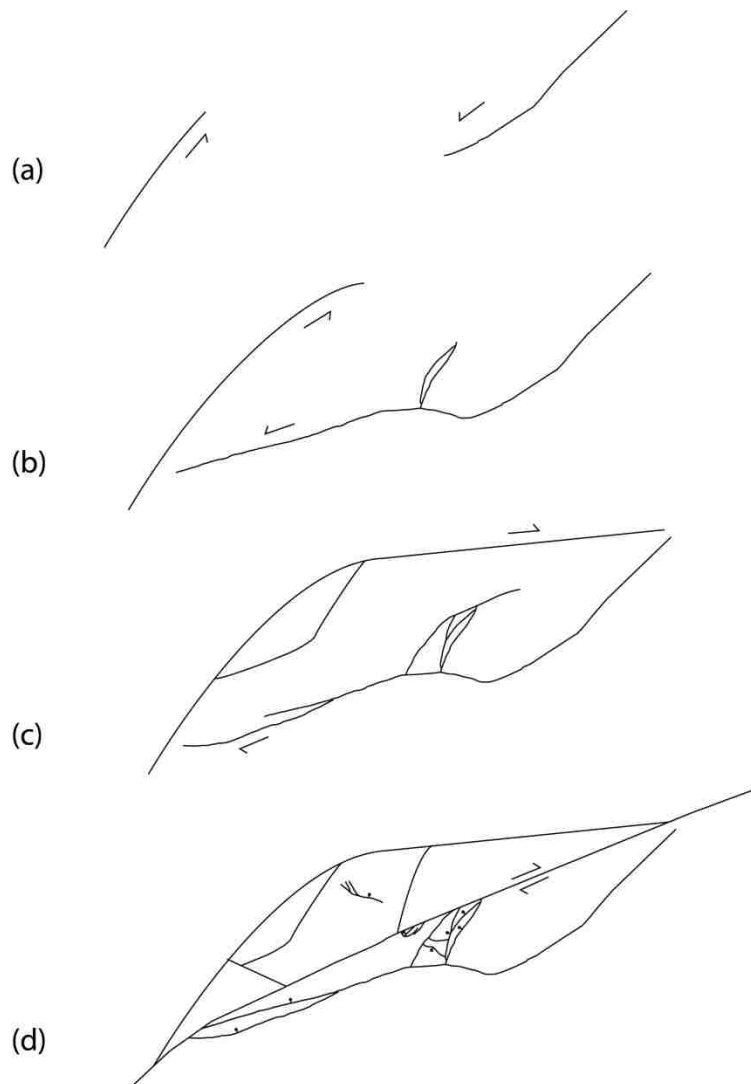


Figure 10. Proposed model of duplex development containing both normal and reverse faults. (a) Two strands of the AMF propagate to the east and the west but at different orientations. (b) The southern, westward propagating fault bends, creating a restraining bend due to changes in lithology at depth. This creates associated reverse faults. (c) The northern, eastward propagating fault bends and forms a releasing bend in response to the fault to the south. Reverse faults continue to form. (d) The AMF breaks through the center of the two fault splays, separating zones of transtension and transpression. In the northern part of the duplex, normal faults form in response to strain accumulation in the duplex

Appendix A

Point counts, fault data and station data

This appendix contains data collected for this project and outlines them in tables. Tables include thin section point counts, fault data and station data.

	15-1	15-3	15-12	15-13	15-14	15-19	15-22
Q	58	15	24	0	2	61	17
S	31	9	31	7	33	6	49
P	0	62	36	89	40	23	30
B	2	7	3	0	9	3	0
H	0	0	0	0	0	0	0
C	5	6	3	2	6	0	0
F							
Oxides	3	1	2	2	11	6	4
TOT	37	57	33	53	26	35	14
Corralation	Kane Wash?	Monotony	Hiko	Harmony	Shingle Pass Int	Leach Canyon	Shingle Pass Lower
Station Num	#51	#52	#68	#72	#73	#82	#102

Table 1. Thin section point counts and their correlated units. Left hand column represents modal percentages of individual minerals. Q = quartz, S = sanidine, P = plagioclase, B = Biotite, H = hornblende, C = clinopyroxene, F = faylite, TOT = total percent phenocrysts. Station number locations are provided on Plate 6.

Stike	Dip	Dip Direction	Slickenlines	Station Number
58	44	N	45 W	#51
61	34	N	45 W	#51
22	44			#51
71	38	N	33 W	#51
46	36	N	30 W	#51
67	61	N		#51
25	27	E		#60
171	23	E		#60
7	30	E		#60
219	44	NW	50 E	#65
63	36	SE	35 E	#65
56	49	NW	Dip Slip	#65
220	40	N	20 E	#65
20	36	E		#65
24	61	SW		#67
128	63	S		#68
78	63	S		#74
85	62	S		#74
35	48	NW	5 N	#75
44	63	SE		#79
20	76	W		#80
85	58	N		#83
156	50	W		#88
148	63	W		#90
85				#90
54				#95
175				#95
25				#101
33	75	W		#103
10	73	E		#104
8	79	W		#106
150	74	NE		#107
9	3	W		#114
164	70	W		#115
81	75	E		#115

Table 2. Fault attitudes. Station locations are provided on Plate 6.

Station Number	Strike	Dip	Dip Direction	Unit	Data Type
7	11	46	E		CF
7	29	21	E		CF
9	149	38	W	Dsl	Bedding
9	150	30	W	Dsl	Bedding
9	154	30	W	Dsl	Bedding
9	164	20	W	Dsl	Bedding
9	167	16	W	Dsl	Bedding
9	141	45	W	Dsl	Bedding
10	34	54	E	Dse?	Bedding
10	22	36	E	Dse?	Bedding
10	10	39	E	Dse?	Bedding
10	10	38	E	Dse?	Bedding
11	162	26	W		Bedding
11	29	4	W		Bedding
12	179	20	W	Dse or Sl	Bedding
12	180	18	W	Dse or Sl	Bedding
12	170	14	W	Dse or Sl	Bedding
12	165	16	W	Dse or Sl	Bedding
12	16	19	W	Dse or Sl	Bedding
14	106	16	S		
14	155	17	W		
16	5	30	E	Tsp	CF
16	162	25	E	Tsp	CF
16	5	25	E	Tsp	CF
18	2	37	E	Tsp	CF
23	162	28	W	Dolomite	Bedding
23	0	12	W	Dolomite	Bedding
24	155	35	W	Dolomite	Bedding
25	176	22	W	Dolomite	Bedding
25	174	17	W	Dolomite	Bedding
27	65	24	SE	Tp	CF
28	140	22	S	Dsi	Bedding
29	167	39	E	Thh	CF
30	170	54	E	Thh	CF
31	174	44	E	Thh	CF
33	10	33	E	Tp	CF
34	22	27	E	Tsp	CF
35	174	28	E	Tsp	CF
36	113	10	S	Dse	Bedding

Table 3. Data measured or denoted at each station. Strike and dip, unit and data type are shown for each station. Station locations are provided on Plate 6.

Station Number	Strike	Dip	Dip Direction	Unit	Data Type
37	10	25	W	Dse	Bedding
38	170	29	SW	Dse	Bedding
39	157	24	SW	Dse	Bedding
40	160	20	W	Dse	Bedding
41	158	17	W	Dse	Bedding
42	130	20	SW	Dse	Bedding
43	142	6	W	Dse	Bedding
44	136	15	W	Dse	Bedding
45	141	14	SW	Dse	Bedding
46	152	25	SW	Dse	Bedding
47	146	20	SW	Dse	Bedding
48	162	25	W	Dse	Bedding
49	115	28	W	Dse	Bedding
50	165	22	W	Dse	Bedding
51	146	25	W	Dse	Bedding
56	154	34	S	Thh	CF
57	10	40	E	Th	CF
58	137	21	W	Dse	Bedding
59	120	85	W	Th	CF
60	132	73	SE	Thh	CF
61	62	34	SE	Th	CF
62	155	30	E	Th	CF
63	170	29	E	Th	CF
64	154	22	E	Th	CF
65	38	26	E	Th	CF
66	53	34	W	Th	CF
67	7	24	E	Th	CF
68	136	37	E	Th	CF
69	136	14	E	Th	CF
70	148	38	E	Th	CF
71	4	20	E	Th	CF
72	173	15	E	Th	CF
73	135	36	E	Th	CF
74	66	24	NE	Th	CF
75	16	42	E	Th	CF
76	74	28	E	Th	CF
78	55	26	NE	Tks	CF
79	121	20	W	Dse	Bedding
80	172	24	W	Dse	Bedding
81	143	19	W	Dse	Bedding
82	125	16	W	Dse	Bedding

Table 3 (continued). Station data. Strike and dip, unit and data type are shown for each station.

Station Number	Strike	Dip	Dip Direction	Unit	Data Type
83	119	20	W	Dse	Bedding
84	117	11	NW	Dse	Bedding
85	164	16	W	Dse	Bedding
86	145	18	W	Dse	Bedding
87	137	12	W	Dse	Bedding
88	137	12	W	Dse	Bedding
89	72	25	W	Oes	Bedding
90	111	33	S	Oes	Bedding
91	102	25	S	Oes	Bedding
92	66	18	SE	Oes	Bedding
93	146	28	S	DI or Oes	Bedding
94	143	12	S	Dse	Bedding
95	151	11	S	Dse	Bedding
96	138	14	SE	Dse	Bedding
97	128	15	E	Dse	Bedding
98	146	13	SE	Dse	Bedding
99	130	16	SE	Dse	Bedding
100					
101	150	26	NW	Oeq	Bedding
102	113	12	NE	Oeq	Bedding
103	30	12	NE	TKs	Bedding
104	131	21	SW		
105	6	35	E	TKs	Bedding
106	25	19	SW	TKs	Bedding
107	164	36	NE	?	CF
108					
109					
110					AMF-25 ME-1
111	130	41	N	Tm	CF
112					
113					
114				Tsp	
115					
116	77	20	S	Tsp	CF
117	11	29	E	Tsp	CF
#1					
#2					
#3	177	36	E	Tsp	CF
#4	49	62	E	Tp?	CF
#5					
#6	173	31	E	Thh	CF

Table 3 (continued). Station data. Strike and dip, unit and data type are shown for each station.

Station Number	Strike	Dip	Dip Direction	Unit	Data Type
#6	173	31	E	Thh	CF
#6	26	30	E	Thh	CF
#6	146	32	E	Thh	CF
#7	15	32	E	Thh	CF
#8	0	26	E	Th	CF
#8	19	35	E	Th	CF
#8	169	9	E	Th	CF
#9				?	
#11	1	15	E	Th	CF
#11	135	15	E	Th	CF
#11	48	16	E	Th	CF
#12	15	16	E	Th	CF
#13	141	26	NE	Th	CF
#14	2	36	E	Th	CF
#16	34	39	E	Th	CF
#16	26	24	E	Th	CF
#17	137	35	N	Th	CF
#18	149	51	E	Th	CF
#20	155	41	E	Th	CF
#20	24	16	E	Th	CF
#21	95	50	E	Th	CF
#21	15	26	NE	Th	CF
#22	23	33	SE	Tk1	CF
#22	10	35	E	Th	CF
#24	116	24	S	Oes	Bedding
#25	46	34	S	TKs	Bedding
#26	10	10	E	Tks	Bedding
#27	22	40	E	Tsp	CF
#27	46	34	E	Tm	CF
#28	18	30	E	Tsp	CF
#29	167	49	SW	Red Congl	Bedding
#30	5	26	E	Unnamed I	Bedding
#32	60	36	E	Tsp	CF
#33	52	20	SE	Tsp	CF
#34	8	54	E	Tsp	CF
#36	155	26	NE	Tp?	CF
#37	11	55	E	Th	CF
#38	15	28	E	Tm	CF
#39	168	36	NE	Tsp	CF
#41	22	45	NE	Th	CF

Table 3 (continued). Station data. Strike and dip, unit and data type are shown for each station.

Station Number	Strike	Dip	Dip Direction	Unit	Data Type
#41	359	31	E	Th	CF
#42	172	34	E	Th	CF
#42	100	40	E	Th	CF
#43	120	34	N	Th	CF
#43	175	39	N	Th	CF
#44	8	47	E	Th	CF
#44	165	22	E	Th	CF
#44	112	25	E	Th	CF
#45	136	39	NE	Th	CF
#47	21	51	E	Tk2	CF
#47	26	38	E	Tk2	CF
#47	9	21	E	Tk2	CF
#48	54	46	N	Th	CF
#48	74	30	E	Th	CF
#49	11	16	E	Th	CF
#50	10	14	E	Th	CF
#51					
#52					
#53					
#53					
#54					
#55					
#56	314	13	SW	Oes	Bedding
#57					
#56					
#59					
#60	38	31	E	Freshwate	Bedding
#61					
#62					
#63	22	16	E		Bedding
#64	10	20	E	Tsp	CF
#64	162	7	E	Tsp	CF
#65	163	21	E	Thh	CF
#66	39	31	E	Thh	CF
#67	51	14	E	Th	CF
#67	24	29	NE	Qoa	Bedding
#68	163	58	E	?	CF
#68	173	71	E	?	CF
#69	160	55	E	?	CF

Table 3 (continued). Station data. Strike and dip, unit and data type are shown for each station.

Station Number	Strike	Dip	Dip Direction	Unit	Data Type
#70	174	42	E	?	CF
#71	148	43	E	?	CF
#72	127	40	NE	Thh?	CF
#73	176	30	E	Condor? T	CF
#74				Fault	
#75				Fault	
#76				AMF-ME 15-15	
#77				Pinkish red tuff, breaks in blocks	
#78	154	40	NE	Same as #	CF
#79	138	54	NW	Same as #	CF
#80				Fault	
#81	102	76	N	?	CF
#81	65	36	N	?	CF
#81	92	54	N	Grey oran	CF
#81	82	43	N	Grey oran	CF
#82					
#83					
#84	48	54	NW	Grey oran	CF
#85	177	36	E	Th	CF
#86	174	30	E	Th	CF
#87	6	54	E	Th	CF
#88	12	52	E	Th	CF
#89	164	42	E	Th	CF
#90	12	43	E	Th	CF
#90	2	30	E	Th	CF
#91	172	58	E	Th	CF
#91	5	47	E	Th	CF
#92	20	52	E	Th	CF
#92	24	60	E	Th	CF
#92	24	67	E	Th	CF
#93	14	43	E	Th	CF
#93	6	52	E	Th	CF
#94	165	33	E	Th	CF
#95	170	30	E	?	
#95	170	33	E	?	
#96	177	23	E	Th	CF
#96	126	34	NE	Th	CF
#96	18	19	E	Th	CF
#97	168	27	E	Th	CF
#98	19	47	E	Th	CF
#98	68	15	E	Th	CF

Table 3 (continued). Station data. Strike and dip, unit and data type are shown for each station.

Station Number	Strike	Dip	Dip Direction	Unit	Data Type
#98	68	15	E	Th	CF
#99	123	24	NE	Thh	CF
#99	17	33	E	Th	CF
#100	137	24	NE	Tk2	CF
#100	154	58	NE	Tk2	CF
#101	164	40	E	Tk2	CF
#101	167	65	E	Tk2	CF
#102	170	43	E	Tk2?	CF
#102	9	55	E	?	CF
#103	179	40	E	Th	CF
#103	160	44	E	Th	CF
#105	2	45	E	Th	CF
#105	15	48	E	Th	CF
#105	44	40	SE	Th	CF
#105	15	44	E	Th	CF
#105	42	42	SE	Th	CF
#106	12	70	W	Th	CF
#108	29	34	E	Thh	CF
#109	4	37	E	Thh	CF
#110	146	65	NE	Th	CF
#110	88	16	S		CF
#11	161	34	NE	Th	CF
#11	173	16	E	Th	CF
#112	160	35	E	Th	CF
#112	49	39	SE	Thh	CF
#112	141	21	E	Th	CF
#113	165	46	E	Tk2	CF
#116	116	25	E	Tk1	CF
#117	33	36	S	Tm	CF
#118	8	25	NE	Th	CF
#119	165	45	W	Tm	CF

Table 3 (continued). Station data. Strike and dip, unit and data type are shown for each station.

Appendix B

Geochronology

Samples analyzed by the $^{40}\text{Ar}/^{39}\text{Ar}$ method at the University of Nevada Las Vegas were wrapped in Al foil and stacked in 6 mm inside diameter sealed fused silica tubes. Individual packets averaged 3 mm thick and neutron fluence monitors (GA-1550 biotite) were placed every 5-10 mm along the tube. Synthetic K-glass and optical grade CaF_2 were included in the irradiation packages to monitor neutron induced argon interferences from K and Ca. Loaded tubes were packed in an Al container for irradiation. Samples irradiated at the U. S. Geological Survey TRIGA Reactor, Denver, CO were in-core for 20 hours in the In-Core Irradiation Tube (ICIT) of the 1 MW TRIGA type reactor. Correction factors for interfering neutron reactions on K and Ca were determined by repeated analysis of K-glass and CaF_2 fragments. Measured $(^{40}\text{Ar}/^{39}\text{Ar})_{\text{K}}$ values were $4.1 (\pm 58.54\%) \times 10^{-3}$. Ca correction factors were $(^{36}\text{Ar}/^{37}\text{Ar})_{\text{Ca}} = 2.55 (\pm 3.50\%) \times 10^{-4}$ and $(^{39}\text{Ar}/^{37}\text{Ar})_{\text{Ca}} = 6.97 (\pm 3.69\%) \times 10^{-4}$. J factors were determined by fusion of 4-8 individual crystals of GA-1550 biotite neutron fluence monitors which gave reproducibility's of 0.3% to 0.8% at each standard position. Variation in neutron fluence along the 100 mm length of the irradiation tubes was <4%. Matlab curve fit was used to determine J and uncertainty in J at each standard position. No significant neutron fluence gradients were present within individual packets of crystals as indicated by the excellent reproducibility of the single crystal GA-1550 biotite fluence monitor fusions.

Irradiated GA-1550 biotite standards together with CaF_2 and K-glass fragments were placed in a Cu sample tray in a high vacuum extraction line and were fused using a 20 W CO_2 laser. Sample viewing during laser fusion was by a video camera system

and positioning was via a motorized sample stage. Samples analyzed by the furnace step heating method utilized a double vacuum resistance furnace similar to the Staudacher et al. (1978) design. Reactive gases were removed by three GP-50 SAES getters prior to being admitted to a MAP 215-50 mass spectrometer by expansion. The relative volumes of the extraction line and mass spectrometer allow 80% of the gas to be admitted to the mass spectrometer for laser fusion analyses and 76% for furnace heating analyses. Peak intensities were measured using a Balzers electron multiplier by peak hopping through 7 cycles; initial peak heights were determined by linear regression to the time of gas admission. Mass spectrometer discrimination and sensitivity was monitored by repeated analysis of atmospheric argon aliquots from an on-line pipette system. Measured $^{40}\text{Ar}/^{36}\text{Ar}$ ratios were $279.23 \pm 0.46\%$ during this work, thus a discrimination correction of 1.0583 (4 AMU) was applied to measured isotope ratios. The sensitivity of the mass spectrometer was $\sim 6 \times 10^{-17}$ mol mV⁻¹ with the multiplier operated at a gain of 36 over the Faraday. Line blanks averaged 1.69 mV for mass 40 and 0.02 mV for mass 36 for laser fusion analyses. Discrimination, sensitivity, and blanks were relatively constant over the period of data collection. Computer automated operation of the sample stage, laser, extraction line and mass spectrometer as well as final data reduction and age calculations were done using LabSPEC software written by B. Idleman (Lehigh University). An age of 98.50 Ma (Spell and McDougall, 2003) was used for the GA-1550 biotite fluence monitor in calculating ages for samples.

For $^{40}\text{Ar}/^{39}\text{Ar}$ analyses a plateau segment consists of 3 or more contiguous gas fractions having analytically indistinguishable ages (i.e. all plateau steps overlap in age at $\pm 2\sigma$ analytical error) and comprising a significant portion of the total gas released (typically >50%). Total gas (integrated) ages are calculated by weighting by the amount of ^{39}Ar released, whereas plateau ages are weighted by the inverse of the variance. For each sample inverse isochron diagrams are examined to check for the effects of excess argon. Reliable isochrons are based on the MSWD criteria of Wendt and Carl (1991) and, as for plateaus, must comprise contiguous steps and a significant fraction of the total gas released. All analytical data are reported at the confidence level of 1σ (standard deviation).

Crystal	T (°C)	t (min.)	³⁶ Ar	³⁷ Ar	³⁸ Ar	³⁹ Ar	⁴⁰ Ar	% ⁴⁰ Ar*	Ca/K	⁴⁰ Ar*/ ³⁹ Ar	Age (Ma)	1s.d.
1	1600	2	0.021	0.062	0.018	1.508	5.925	73.7	0.28007	2.10684	18.72	1.41
2	1600	2	0.021	0.134	0.013	0.599	4.464	53.5	1.52441	1.61332	14.35	2.29
3	1600	1	0.045	0.269	0.057	3.450	15.313	42.8	0.53118	1.71900	15.29	1.35
4	1600	1	0.038	0.065	0.038	1.724	10.754	35.3	0.25684	1.88960	16.80	2.66
5	1600	1	0.031	0.185	0.057	2.440	8.049	38.9	0.51653	1.02981	9.17	1.31
6	1600	1	0.028	0.238	0.039	2.476	10.249	64.5	0.65487	2.26610	20.12	1.89
7	1600	1	0.029	0.056	0.016	0.829	5.513	12.5	0.46019	0.58707	5.24	1.98
8	1600	1	0.027	0.134	0.085	5.484	13.819	77.0	0.16645	1.72871	15.37	0.35
9	1600	1	0.111	0.159	0.095	4.222	34.701	20.5	0.25654	1.62799	14.48	0.41
10	1600	1	0.149	0.031	0.034	0.329	39.356	2.1	0.64193	2.50811	22.26	8.57
11	1600	1	0.406	0.056	0.093	1.348	110.836	0.5	0.28300	0.37873	3.38	7.09
12	1600	1	0.019	0.093	0.025	1.632	5.375	85.0	0.38820	1.95494	17.37	0.72
13	1600	1	0.167	0.079	0.065	2.324	46.417	4.2	0.23156	0.80292	7.16	1.32
									Mean ± s.d. =		13.82	5.62
									Wtd mean age =		15.13	0.42
									(8 fusions)			
									No isochron			
note: isotope beams in mV rlsd = released, error in age includes J error, all errors 1 sigma												
(36Ar through 40Ar are measured beam intensities, corrected for decay in age calculations)												

Table 4. ⁴⁰Ar/³⁹Ar data from sample of Kane Wash Tuff.

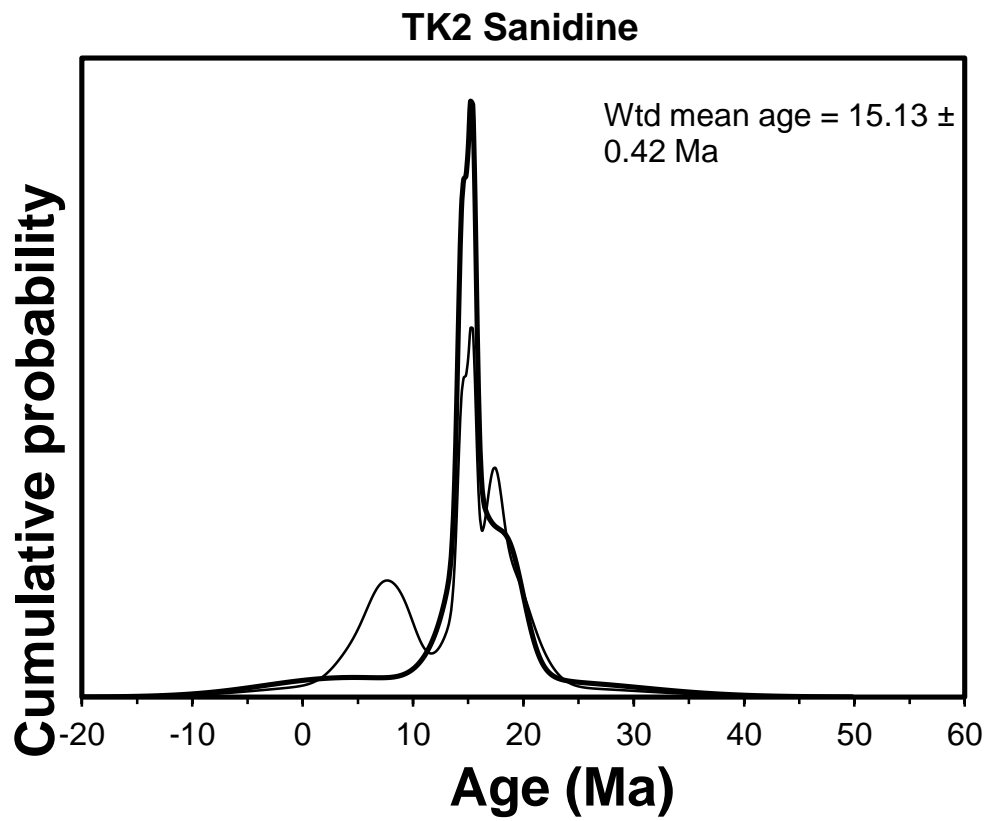


Fig 1b. Probability graph showing the probability of the given age based on the samples measured. It shows the highest probability of the mean age to be 15.13 ± 0.42 Ma.

Appendix C

Plates

Plate 1. Geologic map of the Arrowhead Mine Fault, (Please find the attachment entitled Geologic Map of the Arrowhead Mine Fault, Lincoln County, Nevada).

Plate 2. Cross sections of the Arrowhead Mine Fault (Please find the attachment entitled Cross Sections).

Plate 3. Fault timing of the Arrowhead Mine Fault (Please find the attachment entitled Fault Timing of the Arrowhead Mine Fault, Lincoln County, Nevada).

Plate 4. Fence diagram of the Arrowhead Mine Fault (Please find the attachment entitled Fence Diagram).

Plate 5. Retrodeformation of cross section B-B' (Please find the attachment entitled Retrodeformation).

Plate 6. Station map showing where data was collected (Please find the attachment entitled Station Map).

References

- Abdelhaleem, S., 2015, Kinematics and Timing of the Miocene-Quaternary Deformation in Nellis Dunes Recreation Area: UNLV Thesis, Dissertations, Professional Papers, and Capstones 2798, p. 1-83.
- Anderson, R.E., compiler, 1999, Fault number 1122, Maynard Lake fault, in Quaternary fault and fold database of the United States: U.S. Geological Survey website, <http://earthquakes.usgs.gov/hazards/qfaults>, accessed 06/27/2016 03:26 PM).
- Anderson, R.E., compiler, 1999, Fault number 1122, Maynard Lake fault, in Quaternary fault and fold database of the United States: U.S. Geological Survey website, <http://earthquakes.usgs.gov/hazards/qfaults>, accessed 06/27/2016 03:26 PM)
- Anderson, R.E., Felger, T.J., Diehl, S.F., Page, W.R., and Workman, J.B., 2010, Integration of tectonic, sedimentary, and geohydrologic processes leading to a small-scale extension model for the Mormon Mountains area north of Lake Mead, Lincoln County, Nevada: Special Paper of the Geological Society of America, v. 463, p. 395–426, doi: 10.1130/2010.2463(18).
- Atwater, T., 1970. Implications of plate tectonics for the Cenozoic tectonic evolution of western North America. Geological Society of America Bulletin, 81(12), p.3513-3536.
- Axen, G.J., 1998, The Caliente-Enterprise zone, southeastern Nevada and southwestern Utah: Geological Society of America Special Paper 323, p 181-194.
- Axen, G.J., Wernicke, B.P., Skelly, M.F. and Taylor, W.J., 1990. Mesozoic and Cenozoic tectonics of the Sevier thrust belt in the Virgin River Valley area, southern Nevada: Geological Society of America Memoirs, 176, p.123-154.
- Axen, G.J., Taylor, W.J. and Bartley, J.M., 1993. Space-time patterns and tectonic controls of Tertiary extension and magmatism in the Great Basin of the western United States: Geological Society of America Bulletin, 105, p.56-76.
- Best, M.G. and Christiansen, E.H., 1991. Limited extension during peak Tertiary volcanism, Great Basin of Nevada and Utah. Journal of Geophysical Research: Solid Earth, 96(B8), p.13509-13528.
- Best, M.G., Christiansen, E.H., de Silva, S. and Lipman, P.W., 2016. Slab-rollback ignimbrite flareups in the southern Great Basin and other Cenozoic American arcs: A distinct style of arc volcanism: Geosphere, v. 12, no. 4, p.1097-1135.
- Best, M.G., Scott, B., Rowley, P.D., Swadley, W.C., Anderson, R.E., Gromme, S.C., Harding, A.E., Deino, A.L., Christiansen, E.H., Tingey, D.G., and Sullivan, K.R., 1993, Crustal Evolution of the Great Basin and the Sierra Nevada: Field Trip Guidebook for the 1993 Joint Meeting of the Cordilleran/Rocky Mountain Sections of the Geological Society of America, Reno, Nevada, p. 285-381.

- Best, M.G., Christiansen, E.H., and Gromme, S., 2013a, Introduction: The 36-18 Ma southern Great basin, USA, ignimbrite province and flareup: Swarms of subduction-related supervolcanoes: *Geosphere*, v. 9, no. 2, p. 260-283.
- Best, M.G., Christiansen, E.H., Deino, A.L., Gromme, S., Hart, G.L., and Tingey, D.G., 2013b, The 36-18 Ma Indian Peak-Caliente ignimbrite field and calderas, southeastern Great basin, USA: Multicyclic super-eruptions: *Geosphere*, v. 9, no. 4, p. 864-950.
- Best, M.G., Christiansen, E.H., Deino, A.L., Gromme, S., Hart, G.L., Tingey, D.G., 2013c, The 36-18 Ma Central Nevada ignimbrite field and calderas, Great Basin, USA; Multicyclic super-eruptions: *Geosphere*, v. 9, no. 6, p. 1562-1636.
- Bidgoli, T.S., Stockli, D.F., and Walker, J.D., 2015, Low-temperature thermochronologic constraints on the kinematic histories of the Castle Cliffs, Tule Springs, and Mormon Peak detachments, southwestern Utah and southeastern Nevada: *Geosphere*, v. 11, p. 850-867.
- Bull, W.B. and McFadden, L., 1977, Tectonic Geomorphology of North and South of the Garlock Fault, California. In: Dohring, D.O., Ed., *Geomorphology in Arid Regions*, Publ. in *Geomorphology*, State University of New York, Binghamton, p. 115-138.
- Cook, E.F., 1965, Stratigraphy of Tertiary volcanic rocks in eastern Nevada: Nevada Bureau of Mines Report 11, 61 p.
- Cembrano, J., González, G., Arancibia, G., Ahumada, I., Olivares, V. and Herrera, V., 2005. Fault zone development and strain partitioning in an extensional strike-slip duplex: A case study from the Mesozoic Atacama fault system, Northern Chile: *Tectonophysics*, v. 400, p.105-125.
- DeCelles, P.G. and Coogan, J.C., 2006. Regional structure and kinematic history of the Sevier fold-and-thrust belt, central Utah: *Geological Society of America Bulletin*, v. 118, p. 841-864.
- dePolo and dePolo., 2012, Earthquakes in Nevada: 1840s to 2010: Nevada Bureau of Mines and Geology Map 179,1 plate.
- Dickinson, W.R., 2006. Geotectonic evolution of the Great Basin: *Geosphere*, v. 2, no. 7, p. 353-368.
- Ekren E.B., Orkild P.P., Sargent K.A., and Dixon G.L., Geologic map of Tertiary rocks, Lincoln County, Nevada: USGS IMAP 1041, scale 1: 250000 .
- Faulds, J., and Varga, R., 1998, The role of accommodation zones and transfer zones in the regional segmentation of extended terranes: *Geological Society of America Special Paper 323*, p. 1-45.
- Faulds, J.E., Henry, C.D. and Hinz, N.H., 2005. Kinematics of the northern Walker Lane: An incipient transform fault along the Pacific–North American plate boundary: *Geology*, v. 33, p. 505-508.

- Fryxell, J.E., 1991. Tertiary tectonic denudation of an igneous and metamorphic complex, west-central Grant Range, Nye County, Nevada. *Geology and Ore Deposits of the Great Basin: Symposium and Proceedings: Reno, Nevada, Geological Society of Nevada*, p. 87-92.
- Guth, P.L., 1981. Tertiary extension north of the Las Vegas Valley shear zone, Sheep and Desert Ranges, Clark County, Nevada. *Geological Society of America Bulletin*, 92, p.763-771.
- Guth P., 1990. Superposed Mesozoic and Cenozoic deformation, Indian Springs Quadrangle, southern Nevada, in *Basin and Range Extensional Tectonics Near the Latitude of Las Vegas, Nevada: Geological Society of America Memoir 176*, p. 237-249.
- Guth, P.L., Schmidt, D.L., Deibert, J. and Yount, J.C., 1988. Tertiary extensional basins of northwestern Clark County, Nevada. in *This Extended Land—Geological Journeys in the Southern Basin and Range: Geological Society of America, Cordilleran Section, Field Trip Guidebook*, p. 239-254.
- Hudson, M.R., Rosenbaum, J.G., Gromme, C.S., Scott, R.B., and Rowley, P.D., 1998, Paleomagnetic evidence for counterclockwise rotation in a broad sinistral shear zone, Basin and Range province, southeastern Nevada and southwestern Utah: *Geological Society of America Memoir 176*, p. 213-236.
- Jayko, A.S., 1990. Shallow crustal deformation in the Pahrangat area, southern Nevada: *Geological Society of America Memoir 176*, p. 213-234.
- Jayko, A.S., 2007, *Geologic Map of the Pahrangat Range 30'x60' Quadrangle, Lincoln and Nye Counties, Nevada, Scale 1:100,000*.
- Jensen, E., Cembrano, J., Faulkner, D., Veloso, E. and Arancibia, G., 2011. Development of a self-similar strike-slip duplex system in the Atacama Fault system, Chile: *Journal of Structural Geology*, v. 33, p.1611-1626.
- Jones, C.H., Wernicke, B.P., Farmer, G.L., Walker, J.D., Coleman, D.S., McKenna, L.W. and Perry, F.V., 1992. Variations across and along a major continental rift: An interdisciplinary study of the Basin and Range Province, western USA: *Tectonophysics*, 213, p.57-96.
- Kreemer, C., Belwitt, G., and Bennett, R., 2010, Present-day motion and deformation of the Colorado Plateau: *Geophysical Research Letters*, v. 37, p. 1-5.
- Lerch, D. W., Klemperer, S. L., Glen, J. M. G., Ponce, D. A., Miller, E. L., and Colgan, J. P., 2007, Crustal structure of the northwestern Basin and Range Province and its transition to unextended volcanic plateaus: *Geochemistry, Geophysics, Geosystems*, v. 8, p.621-638.

- Long, S.P., 2012. Magnitudes and spatial patterns of erosional exhumation in the Sevier hinterland, eastern Nevada and western Utah, USA: Insights from a Paleogene paleogeologic map: *Geosphere*, v. 8, p. 881-901.
- Long, S.P., Henry, C.D., Muntean, J.L., Edmondo, G.P. and Cassel, E.J., 2014. Early Cretaceous construction of a structural culmination, Eureka, Nevada, USA: Implications for out-of-sequence deformation in the Sevier hinterland: *Geosphere*, 10, p.564-584.
- Mitchell, T.M. and Faulkner, D.R., 2009. The nature and origin of off-fault damage surrounding strike-slip fault zones with a wide range of displacements: a field study from the Atacama fault system, northern Chile. *Journal of Structural Geology*, v. 31, no. 8, p. 802-816.
- Muhammad, M.M., 2016, Structural Evolution of the Maynard Lake Fault within the Left-Lateral Pahrnagat shear zone, Nevada, USA: UNLV Thesis, Dissertations, Professional Papers, and Capstones 2798, p. 1-79, 2 plates.
- Naylor, M.A., Mandl, G.T. and Supesteijn, C.H.K., 1986. Fault geometries in basement-induced wrench faulting under different initial stress states. *Journal of Structural Geology*, 8, p.737-752.
- Novak, S.W., 1984. Eruptive history of the rhyolitic Kane Springs Wash volcanic center, Nevada. *Journal of Geophysical Research: Solid Earth*, 89, p.8603-8615.
- O'Leary, 2000, Tectonic Significance of the Rock Valley Fault Zone, Nevada Test Site *in* Whitney, J.W., Keefer, W.R., eds, *Geologic and Geophysical Characterization Studies of Yucca Mountain, Nevada, A Potential High-Level Radioactive-Waste repository: United States Geologic Survey, –Digital Dsta Series 058, paper I, p. 1-13.*
- Pampeyan, E.H., 1993, Geologic map of the Meadow Valley Mountains, Lincoln and Clark counties, Nevada: USGS Map I-2173, 1:50,000 scale.
- Price, T.G., 2017, Miocene-Pliocene(?) folds and normal faults associated with the left-lateral Buckhorn fault and regional implications, Pahrnagat shear zone, Nevada: UNLV M.S. thesis, 56 pp.
- Rau C. J., and Forsyth D. W., 2011, Melt in the mantle beneath the amagmatic zone, southern Nevada: *Geology*, v. 145, p. 117-152.
- Root, K.G., 1990. Extensional duplex in the Purcell Mountains of southeastern British Columbia: *Geology*, v. 18, p. 419-421.

- Scott, R., Swadley, W.C., Page, W., and Novak, S., 1991, Preliminary Geologic Map of the Gregerson Basin quadrangle, Lincoln County, Nevada. U.S. Geological Survey Open-file Report 90-646, 21, 1 plate, 1:24,000 scale.
- Slemmons, D.B., Jones, A.E. and Gimlett, J.I., 1965. Catalog of Nevada earthquakes, 1852-1960. Bulletin of the Seismological Society of America, 55, p. 519-565.
- Sonder, L., and Jones C., 1999, Western United States extension: How the West was widened: Annual Review of Earth and Planetary Sciences, v. 27, p. 417-462.
- Spell, T.L., McDougall, I., 2003, Characterization and calibration of $^{40}\text{Ar}/^{39}\text{Ar}$ dating standards: Chemical Geology, v. 198, p. 189-211.
- Staudacher, T.H., Jessberger, E.K., Dorflinger, D., and Kiko, J., 1978, A refined ultrahigh-vacuum furnace for rare gas analysis: Journal of Physics E: Scientific Instruments., v. 11, p. 781-784.
- Sylvester, A., 1988, Strike-slip faults: Geological Society of America Bulletin, v. 100, p. 1666-1687.
- Taylor, W.J. and Bartley, J.M., 1992. Prevolcanic extensional Seaman breakaway fault and its geologic implications for eastern Nevada and western Utah: Geological Society of America Bulletin, 104, p.255-266.
- Taylor, W.J., Bartley, J.M., Martin, M.W., Geissman, J.W., Walker, J.D., Armstrong, P.A., and Fryxell, J.E., 2000, Relations between hinterland and foreland shortening: Sevier orogeny, central North American Cordillera: Tectonics, v. 19, p.1124-1143.
- Taylor, W.J., and Switzer, D., 2001, Temporal changes in fault strike (to 90°) and extension directions during multiple episodes of extension: An example from eastern Nevada: Geological Society of America Bulletin, v. 113, p. 743-759.
- Tschanz, C.M., and Pampeyan, E.H., 1970, Geology and mineral deposits of Lincoln County, Nevada: Nevada Bureau of Mines and Geology Bulletin 73, p. 188.
- Wendt, I., and Carl, C., 1991, The statistical distribution of the mean squared weighted deviation: Chemical Geology, v. 86, p. 275-285.
- Wernicke, B., 1992, Cenozoic extensional tectonics of the U.S. Cordillera: Geological Society of America, The Geology of North America, The Cordilleran Orogen: Conterminous U.S., The Decade of North American Geology (DNAG), v. G-3, p. 553-581.
- Wernicke, B., Axen, G.J., and Snow, J.K., 1988, Basin and Range extensional tectonics at the latitude of Las Vegas, Nevada: Geological Society of America Bulletin, v. 100, p.1738-1757.

Woodcock, N.H. and Fischer, M., 1986, Strike-slip duplexes. *Journal of Structural Geology*, v. 8, p.725-735.

Woodcock, N.H. and Rickards, B., 2003, Transpressive duplex and flower structure: Dent fault system, NW England: *Journal of Structural Geology*, 25, p.1981-1992.

Zoback, M.L., Anderson, R.E., and Thompson, G.A., 1981, Cainozoic evolution of the state of stress and style of tectonism of the Basin and Range province of the western United States: *Philosophical Transactions of the Royal Society of London*, v. 300, p. 407-434.

Curriculum Vitae

Michael Evans

MEvansMusic@gmail.com

Structural Geologist

September 2013-Present: UNLV, (Structural Geology) Masters of Geoscience in progress

August 2009-May 2013: California Lutheran University, Thousand Oaks, CA -BS in Geology

September 2005-June 2009: Faith Lutheran High School, Las Vegas, NV

Work Experience

- October 2017- Present: Geologist at Bureau of Land Management
- September 2014- May 2016: Teaching Assistant for Structural Geology at UNLV
- September 2013- May 2014: Graduate Research Assistant at the Applied Geophysics Center at UNLV
- June 2011-August 2012: Research Assistant, Evolutionary and Morphological Trends of Cambrian Agnostid Trilobites- California Lutheran University
- August 2011-May 2013: Geology Departmental Assistant/Teaching Assistant- California Lutheran University.

Field Experience

- Boise State Field camp in Sardinia Italy, 2012 under C.J. Northrup
- Teaching assistant for field based Sedimentology and Stratigraphy projects and field based Structural Geology mapping projects in Rainbow Basin, Ca.
- Mapping of the Arrowhead Mine Fault in the Pahranaagat Shear Zone, Nv as part of masters thesis in Structural Geology.

AWARDS

- Coast Geological Society John Woolley Scholarship- "For Outstanding Achievement in Geological Sciences" 2011
- Recipient of Oaks Academic Award (Academic Scholarship) 2009-2013
- NPGS Research Grant 2013